

THESIS FOR THE DEGREE OF DOCTOR OF PHILOSOPHY

**Water in molecular outflows and shocks:
Studies with Odin and Herschel**

PER BJERKELI



CHALMERS

Department of Earth and Space Sciences
CHALMERS UNIVERSITY OF TECHNOLOGY
Göteborg, Sweden 2012

**Water in molecular outflows and shocks:
Studies with Odin and Herschel**

PER BJERKELI
ISBN 978-91-7385-752-9

© Per Bjerkele, 2012

Doktorsavhandlingar vid Chalmers tekniska högskola
Ny serie Nr: 3433
ISSN 0346-718X
Radio Astronomy & Astrophysics Group
Department of Earth and Space Sciences
Chalmers University of Technology
SE-412 96 Göteborg, Sweden
Phone: +46 (0)31-772 1000

Contact information:

Per Bjerkele
Onsala Space Observatory
Chalmers University of Technology
SE-439 92 Onsala, Sweden

Phone: +46 (0)31-772 5546
Fax: +46 (0)31-772 5590
Email: per.bjerkele@chalmers.se

Cover image:

Left: RGB colour composite showing the velocity structure in the VLA 1623 region. Blue colour is from -50 to 0 km s^{-1} , red is from $+5$ to $+50 \text{ km s}^{-1}$ and green is from 0 to $+5 \text{ km s}^{-1}$.

Right: The 557 GHz spectra toward the same region. This map was presented in Paper III.

Printed by Chalmers Reproservice
Chalmers University of Technology
Göteborg, Sweden 2012

Water in molecular outflows and shocks: Studies with Odin and Herschel

PER BJERKELI

Department of Earth and Space Sciences

Chalmers University of Technology

Abstract

This thesis describes observations and analyses of water in molecular outflows from young stellar objects. The abundance of this molecule (with respect to molecular hydrogen) is deduced from observations carried out primarily with the *Odin* and *Herschel* telescopes. The large spatial extents of molecular outflows allow for mapping observations to be done, but in addition to this, spectroscopy allows for the investigation of the kinematics. The observations discussed in this thesis were acquired over the years 2002 to 2011.

In the first appended research paper, observations of 15 different shocked regions are reported. The targets were primarily molecular outflows, but two supernova remnants were also observed. This study shows that the water abundance in the gas is elevated in the presence of shock waves. Furthermore, the water abundance seems to correlate with the maximum velocity of the shocked gas.

In the second paper, previously published observations of the Herbig-Haro object HH 54 are followed up, using APEX, *Odin* and *Herschel*. In this work we investigate the relative cooling contribution from CO and H₂O and we compare the results with most recent shock models. CO dominates the cooling and we conclude that planar shock models do not explain the observations satisfactorily. Instead we find that a curved geometry can completely account for the observed line profile shapes in the two species. The inferred water abundance is lower than what was previously expected.

In the third paper, *Herschel* mapping observations of VLA 1623 are presented. The ground-state transitions of *o*-H₂O were mapped using the HIFI and PACS instruments but also higher energy transitions were observed towards selected positions in the outflow lobes. The observed H₂O (1₁₀ – 1₀₁) line profiles show a variety of shapes over the observed region and also from this work, we conclude that the water abundance is lower than expected. In addition to this, it is now clear that the regions responsible for the emission in water are warmer than the regions traced by CO. A comparison with H₂ data obtained with *Spitzer* allows us to estimate the physical parameters of the flow. This leads us to conclude, that it does not matter which molecular tracer we use when we infer the force and the power of the VLA 1623 outflow. The analysis is followed up in a letter where we include also the L 1448 and L 1157 outflows.

Keywords: Herbig-Haro objects – ISM:individual objects: HH 54, VLA 1623 – ISM:jets and outflows – ISM:molecules – ISM:abundances – ISM:supernova remnants – stars:formation – stars:pre-main-sequence – stars:winds, outflows

Till Jan och Katerina

List of appended research papers

This thesis is based on the following four publications, referred to by roman numerals in the text.

- I. *Odin observations of water in molecular outflows and shocks*
Bjerkeli, P., Liseau, R., Olberg, M., et al.
Astronomy and Astrophysics 507, 1455 (2009)

- II. *Herschel observations of the Herbig-Haro objects HH 52-54*
Bjerkeli, P., Liseau, R., Nisini, B., et al.
Astronomy and Astrophysics 533, A80 (2011)

- III. *H₂O line mapping at high spatial and spectral resolution*
Herschel observations of the VLA 1623 outflow
Bjerkeli, P. Liseau, R., Larsson, B., et al.
Astronomy & Astrophysics 546, A29 (2012)

- IV. *Physical properties of outflows from Class 0 sources*
Bjerkeli, P. Liseau, R., Rydbeck, G., et al.
Manuscript intended for Astronomy & Astrophysics (2012)

Other publications

I have also participated in the following publications, not included in the thesis. Some of these papers are discussed in the text and are referred to by the name of the leading author(s).

1. *Mapping water in protostellar outflows with Herschel*
PACS and HIFI observations of L1448-C
Nisini, B., Santangelo, G., Antonucci, S., et al.
Astronomy and Astrophysics, in press (2012)

2. *Multi-line detection of O₂ toward ρ Oph A*
Liseau, R., Goldsmith, P. F. , Larsson, B., et al.
Astronomy and Astrophysics 541, A73 (2012)

3. *In-orbit performance of Herschel-HIFI*
Roelfsema, P. R. , Helmich, F. P., Teyssier, D., et al.
Astronomy and Astrophysics 537, A17 (2012)

4. *Water in star-forming regions with the Herschel space observatory (WISH). I. overview of key program and first results*
van Dishoeck, E. F. , Kristensen, L. E. , Benz, A. O., et al.
Publications of the Astronomical Society of the Pacific 123 (900), 138-170 (2011)
5. *Herschel/HIFI detections of hydrides towards AFGL 2591: Envelope emission versus tenuous cloud absorption*
Bruderer, S., Benz, A. O., van Dishoeck, E. F. , et al.
Astronomy and Astrophysics 521, L44 (2010)
6. *Herschel/HIFI spectroscopy of the intermediate mass protostar NGC 7129 FIRS 2*
Johnstone, D., Fich, M., McCoey, C., et al.
Astronomy and Astrophysics 521, L41 (2010)
7. *Herschel/HIFI observations of high-J CO lines in the NGC 1333 low-mass star-forming region*
Yildiz, U. A. , van Dishoeck, E. F. , Kristensen, L. E. , et al.
Astronomy and Astrophysics 521, L40 (2010)
8. *Water in massive star-forming regions: HIFI observations of W3 IRS5*
Chavarría, L., Herpin, F., Jacq, T., et al.
Astronomy and Astrophysics 521, L37 (2010)
9. *Herschel observations of the hydroxyl radical (OH) in young stellar objects*
Wampfler, S. F., Herczeg, G. J. , Bruderer, S., et al.
Astronomy and Astrophysics 521, L36 (2010)
10. *Hydrides in young stellar objects: Radiation tracers in a protostar-disk-outflow system*
Benz, A. O., Bruderer, S., van Dishoeck, E. F., et al.
Astronomy and Astrophysics 521, L35 (2010)
11. *Variations in H_2O^+/H_2O ratios toward massive star-forming regions*
Wyrowski, F., van der Tak, F., Herpin, F., et al.
Astronomy and Astrophysics 521, L34 (2010)

12. *Sensitive limits on the abundance of cold water vapor in the DM Tauri protoplanetary disk*
Bergin, E. A. , Hogerheijde, M. R. , Brinch, C., et al.
Astronomy and Astrophysics 521, L33 (2010)
13. *Water abundances in high-mass protostellar envelopes: Herschel observations with HIFI*
Marseille, M. G. , van der Tak, F. F. S. , Herpin, F., et al.
Astronomy and Astrophysics 521, L32 (2010)
14. *Water in low-mass star-forming regions with Herschel: HIFI spectroscopy of NGC 1333*
Kristensen, L. E. , Visser, R., van Dishoeck, E. F., et al.
Astronomy and Astrophysics 521, L30 (2010)
15. *Water vapor toward starless cores: The Herschel view*
Caselli, P., Keto, E., Pagani, L., et al.
Astronomy and Astrophysics 521, L29 (2010)
16. *Origin of the hot gas in low-mass protostars: Herschel-PACS spectroscopy of HH 46*
van Kempen, T. A., Kristensen, L. E. , Herczeg, G. J. , et al.
Astronomy and Astrophysics 518, L121 (2010)
17. *Water cooling of shocks in protostellar outflows: Herschel-PACS map of L 1157*
Nisini, B., Benedettini, M., Codella, C., et al.
Astronomy and Astrophysics 518, L120 (2010)
18. *Water abundance variations around high-mass protostars: HIFI observations of the DR21 region*
van der Tak, F. F. S. , Marseille, M. G. , Herpin, F., et al.
Astronomy and Astrophysics 518, L107 (2010)
19. *Herschel-PACS spectroscopy of the intermediate mass protostar NGC 7129 FIRS 2*
Fich, M., Johnstone, D., van Kempen, T. A., et al.
Astronomy and Astrophysics 518, L86 (2010)
20. *Stars and gas in the Medusa merger*
Manthey, E., Hüttemeister, S., Aalto, S., Horellou, C., Bjerkele, P.
Astronomy and Astrophysics 490, 975 (2008)

Acknowledgements

There are several people that I want to mention on this page. First of all I would like to express my sincere thanks to my thesis advisor René Liseau. I have had lots of fun over the last five years and you have always been supportive, enthusiastic and available to answer questions. I hope that we can continue to work together for many years to come. I would also like to extend special thanks to John Black, Gustaf Rydbeck, Bengt Larsson and Åke Hjalmarsen for always being helpful and friendly when it comes to questions about everything related to astronomy. Sincere thanks also go to Åke, Magnus, John, Michael, Robert and Per for careful reading of this thesis. Besides this, I would also like to thank Per Bergman for always being there, regardless of whether it is as a teacher, brain, supporter, opponent or moving man.

Other people at Onsala/Chalmers that I want to acknowledge are my fellow Ph.D. students, administrative staff, senior staff and other colleagues that make this place such a nice environment to work in. Some of you, however, deserve to be specially acknowledged. Roger Hammargren was a solid rock during the 20 m observations and has also helped me with many other things. Paula, Katarina K, Katarina N, Maria, Marita and Camilla are always to count on when it comes to administrative matters. Cathy and Alessandro, it was just as fun as you explained to me. With regard to this I would also like to thank Roger, Mats, Magnus and Bosse. To Danne, Fabbe and Frasse, thank you for being such wonderful friends.

To members of WISH and the outflow team but also to the HIFI-ICC I want to express my gratitude. During these years we have had many pleasant meetings and I also enjoyed three months of work at SRON in Groningen. I should perhaps not mention that I am not a frequent user of the Herschel helpdesk. Thank you Carolyn and all other members of the ICC for always answering promptly to any questions related to Herschel-HIFI.

There are also a number of other people I want to mention for various reasons. Many thanks to Barbro & Pelle, Kalle & Jakob, Johan and Thommy. I would also like to take this opportunity to thank my former competitors in the ski tracks, now members of the Bunkeflo Ski Team.

Finally I want to thank my family. You have always been supportive and a source of inspiration. To Elsa, thank you for reminding me about the importance of the Moon when I try to explain my work. And Pernilla, thank you for joining me in this journey and for constantly challenging my intellect. Life is simply a lot more fun together with you!

Per

Contents

Abstract	iii
List of appended papers	vii
Other publications	vii
Acknowledgements	xi
1 Introduction	1
1.1 This thesis	2
1.2 The Interstellar Medium	3
1.2.1 Molecules	3
1.2.2 Dust	4
1.2.3 Magnetic fields	5
1.3 Excitation and de-excitation	6
1.3.1 Rotational transitions	6
1.3.2 Rotational transition strength	8
1.4 Radiative transfer	10
1.4.1 The radiative transfer equation	10
1.4.2 Statistical equilibrium	13
1.5 Radiative transfer analysis	13
1.5.1 Thermal equilibrium	14
1.5.2 Non-thermal equilibrium	15
2 Low-mass star formation	19
2.1 Gravitational collapse	19
2.2 Protostellar formation	20
2.2.1 Classification of young stellar objects	21
2.3 Observing the star formation process	23
3 Molecular outflows	25
3.1 Properties of outflows from low-mass objects	26
3.1.1 Shocks	28
3.1.2 Origin of outflows and ejection mechanisms	29

3.2	Molecules in outflows	30
3.2.1	CO	30
3.2.2	H ₂ O	31
3.2.3	H ₂	32
3.3	Line profile shapes	33
3.3.1	Observed line profiles	33
3.3.2	Predicted line profiles from shock-models	34
3.4	Individual objects	35
3.4.1	HH54	35
3.4.2	VLA 1623	36
4	Appended papers	39
4.1	Introduction	39
4.1.1	Paper I	39
4.1.2	Paper II	40
4.1.3	Paper III	40
4.1.4	Paper IV	41
4.2	Conclusions and summary of the results	41
4.3	Observations and data reduction methods	44
4.3.1	Odin	44
4.3.2	Herschel	44
4.3.3	Data reduction methods	46
4.4	Current and future research projects	46
4.4.1	Herschel observations of the shocked gas in HH 54	46
4.4.2	H ₂ O mapping of the ρ Ophiuchi A cloud	47
	References	49
	Paper I	55
	Paper II	73
	Paper III	91
	Paper IV	107

Introduction

Our solar system has been present for billions of years but for a very long time it was unrecognised by humans. Up until four hundred years ago only a handful of individuals saw it as likely that the planets orbit the Sun. Although the idea of a heliocentric system was presented already two millennia ago by people like Aristarchus of Samos, it was not until the Copernican revolution that this view started to become generally accepted. The invention of the telescope and the work carried out by Galileo Galilei, Johannes Kepler and Sir Isaac Newton gradually changed the general opinion towards the heliocentric view. At that time, observations of the universe were limited to visible wavelengths, i.e., the wavelength region where most of the light originates from stars. The space in between is, however, not at all empty but consists of gas, dust and ices that in most cases are invisible to the human eye. This component, known as the Interstellar Medium (ISM), has been carefully investigated over the last decades, not least through the development of radio- and infrared astronomy.

It is well known that star formation has been ongoing for a long time in the Galaxy and is still occurring (see e.g. Ambartsumian 1947, 1955; Spitzer 1949). It is also known that interstellar clouds in the ISM play a key role in this process. On the other hand, the details behind these processes are not understood to the same extent. For many reasons, it is important to understand how structures like the solar system form. In this context, water has a significant role when interstellar gas turns into stars. A large fraction of the interstellar oxygen is thought to be locked up in the form of water molecules, and as such it has been expected that it serves as an important coolant. A collapsing cloud that eventually forms stars must at some time cool down. Furthermore, water has been shown to be a good tracer of the relatively warm gas that is associated with star forming regions.

When studying the star formation process, one also wants to understand the processes leading to the formation of the molecules that are present in the solar system (and elsewhere) today. The limited knowledge we have of how life emerged on Earth

is a problem as we seek to understand how the conditions for life arose. Nevertheless, we know from the available evidence that life seems to be dependent on the presence of water.

1.1 This thesis

The time that elapses between when a star is “born” and when it “dies” can be billions of years. The time it takes for the star to form constitutes, however, only a very short period of time compared to the stellar lifetime. Of all the stars that are situated in the solar neighbourhood at a given time, it is thus only a small proportion, which is in the formation stage. Even if this time is comparatively short, a lot of important chemistry and physics occur, which will eventually define the newly formed planetary system.

The star formation process is often revealed through observations of outflows that can extend up to parsec scale distances from the central source. Although the ejection mechanisms of these mass-loss phenomena are not fully understood, the formation of outflows seems to be tightly linked to young stellar systems of different masses. Being one of the most studied fields in star formation, outflows seem to be a ubiquitous phenomenon that is necessary in order to form stars.

Four research papers that discuss water in molecular outflows, predominantly from low-mass sources, are appended to this thesis. The aim is to clarify the physical and chemical properties of the gas, responsible for the water emission, as well as to improve the understanding of molecular outflows and shocks in general. Observations have been carried out using space-based sub-millimetre facilities such as the *Odin* satellite (Frisk et al. 2003; Nordh et al. 2003) and the *Herschel* Space Observatory (Pilbratt et al. 2010). The ground-state transitions of *ortho*-water and *para*-water, probing the gas at a relatively low temperature, as well as higher water transitions have been observed over the years 2002 to 2011. From these observations we deduce the molecular abundance, allowing for comparison with up to date shock models. Paper I comprises all observations of water in molecular outflows carried out with *Odin*. Paper II and III discuss the water observations carried out with *Herschel* towards two specific objects, HH 54 and VLA 1623 respectively. Paper IV discusses the physical parameters of outflows when different observational methods are used.

The thesis is structured as follows: this chapter provides a brief description of the interstellar medium and it also contains an introduction to molecular physics and radiative transfer analysis. The basic concepts of the star formation process are described in Chapter 2 while molecular outflows are discussed in Chapter 3. A summary of the appended research papers as well as the main conclusions that can be drawn from these publications are presented in Chapter 4. The observational facilities, data reduction methods that have been used, and current and future research projects are also discussed in that chapter.

1.2 The Interstellar Medium

General references:

Stahler & Palla (2005); Tielens (2005)

Stars form from the matter in the ISM and when they are destroyed, processed stellar material is returned into the ISM. Therefore, one has to understand the ISM in order to understand the evolutionary processes of stars. The ISM consists of ionic, atomic and molecular gas as well as ices and dust particles. On average this matter is extremely dilute compared to environments on the Earth. Most of the mass in the ISM is in the form of atomic hydrogen and helium. The fraction of heavier elements is less than a few percent but is increasing over time through nucleosynthesis and supernova explosions. The dense molecular gas at low temperature is more confined to the inner part of the Galaxy close to its mid-plane than the hot dilute atomic gas. It is in these dense molecular environments where gravitational collapse can occur and stars form.

Most material in the ISM is in the form of gas while only $\sim 1\%$ of the mass is in the form of dust. Although dust constitutes a small fraction of the ISM, it plays an important role in the formation of molecules. The main constituent of molecular clouds is H_2 and this molecule can only be formed efficiently on dust grains where the conversion probability from atomic to molecular hydrogen dramatically increases (Hollenbach & Salpeter 1971). The grains are solid particles composed of silicates, graphite and ices. Being efficient absorbers of ultraviolet and visible radiation makes them excellent protection shields for the formation of other molecules and they are also the major contribution to interstellar extinction. The cooling of the grains occurs through collisions with the gas where infrared (IR) photons are emitted when lattice vibrations decay.

The temperature of the gas can be very low in the vicinity of young stars. Therefore, molecules may be frozen out on the dust grains allowing for surface reactions to take place. On the other hand, these environments may also be very hot. Heating by shocks and/or strong radiation fields can cause the molecules to be released from the grains into the gas phase. Thus, grains play an important role in the chemistry of star forming regions and the observed molecular abundances are the result of a complex interplay of chemical reactions in the gas and on the grains.

1.2.1 Molecules

This thesis is focused on observations of molecules (in particular H_2O) in space. Conveniently and due to that molecules emit photons in the sub-millimetre and millimetre regimes, radiation is not significantly affected by the absorption of foreground material. Therefore, many species can be readily observed with ground-based telescopes, although space-based facilities have been commonly used during the last decades.

As of October 2012 more than 170 different molecules have been detected in space, most of them being diatomic (see e.g. The Cologne Database for Molecular Spec-

trosopy¹ and The Astrochymist²). As already mentioned, dust particles act as effective shields to ultraviolet and visible radiation. This effect makes it possible for many molecules to survive in environments such as dense cores (i.e., the sites of star formation) and a very rich chemistry occurs. It should be noted, however, that molecules can also be found in shock-heated regions and in circumstellar envelopes.

Molecules are mainly formed due to gas-phase reactions in cold molecular clouds. However, in regions where the density is high enough, surface reactions on the grains start to play an important role, affecting formation and destruction. In order to observe a certain molecule through emission in spectral lines, the molecule has to be excited. For low temperature clouds this means that low-level rotational transitions are observed. Also, less complicated molecules are easier to detect than larger molecules. For complicated species the number of transitions are higher and thus each spectral line is weaker. H₂ is a simple molecule, however, the lowest excited rotational level is high above the ground state (~500 K) and therefore it is not easily excited in dark clouds. To observe the rotational transitions of H₂ one has to observe hotter environments such as shock heated regions. Also, the lowest purely rotational transition of H₂ is in the mid-IR regime, at a wavelength of 28.2 μm , and therefore difficult to observe with ground-based telescopes. To observe H₂ from the ground one often instead uses the ro-vibrational transition at 2.12 μm probing gas at even higher temperatures. Although difficult to detect, H₂ has in the past years been observed with success in star forming regions using the *Spitzer* space telescope (Werner et al. 2004).

To probe the cold molecular gas, astronomers have instead observed the CO molecule (Wilson et al. 1970) where the lowest excited rotational energy state is situated at an equivalent temperature of only 5.5 K. A drawback when observing this molecule is, however, that the lowest rotational transitions easily become optically thick. For this reason one often uses isotopologues such as ¹³CO. Due to the fact that the binding energy is high and that oxygen is one of the most abundant elements in the ISM (see e.g. Sofia & Meyer 2001), CO has turned out to be the second most abundant molecule after H₂. The abundance of CO relative to H₂ is of the order 10⁻⁴ (see e.g. van Dishoeck & Black 1987).

To understand the formation of molecules, time-dependent chemical reaction networks are simulated in computers. For dark clouds, models of this type must also take into account the effect of grains.

1.2.2 Dust

Dust in the ISM reveals itself in several different ways. Light from stars is absorbed and scattered by the dust, and for that reason distant stars seem redder and less bright than they would otherwise appear. The light can also be polarised due to non-spherical grains present in the galactic magnetic field. Closer to the stars, scattered light can produce reflection nebulae. The cold dust in the ISM is also “visible” by itself due to

¹<http://www.astro.uni-koeln.de/cdms/>

²<http://www.astrochymist.org/>

the fact that it emits continuum radiation in the infrared.

A clue when determining the properties of the grains, which are responsible for these effects, is the observed extinction curve. Observations tell us that the total extinction is highly dependent on the wavelength and roughly inversely proportional to the same quantity, however, with a few distinctive signatures. The clearly most prominent of these is the peak at 220 nm but also weaker signatures are present, e.g., the silicate absorption feature at 10 μm . From comparison with observations it has become evident that the grains are small and are rich in silicates and possibly also in graphite. The sizes of the grains follow a distribution where the number of grains of certain size is proportional to $a^{-3.5}$ (Mathis, Rumpl, & Nordsieck 1977). The relationship tells us that most of the grains are small. On the other hand, the biggest contribution to the mass is due to the larger grains. This model of the size distribution is the most widely used and it is often referred to as the MRN distribution. Of particular interest in the field of molecular chemistry is of course the composition of the outer mantles where molecules can evaporate when temperatures are sufficiently high.

In the mid-IR regime of the electromagnetic spectrum also larger molecules are observed. The features in the IR-bands are due to linked carbon rings known as polycyclic aromatic hydrocarbons (PAH's).

1.2.3 Magnetic fields

In dense star forming regions, magnetic fields are expected to have a strong influence on the structure of the gas and dust. Of particular interest for the work presented in this thesis is shocked regions where the structure of shocks is expected to be dependent on the strength and the orientation of the magnetic field. Magnetic fields can be revealed using several different indirect methods. However, to directly observe the magnetic field one has to rely on the measurements from Zeeman splitting. Unfortunately only a limited number of interstellar clouds have to this date been observed using this technique. These studies have been carried out using different molecular tracers seen either in emission or in absorption, but common for the observations are that mostly large, low-density clouds have been observed. Magnetic fields are expected to scale with the density to the power of 2/3 when densities are higher than 300 cm^{-3} (Crutcher et al. 2010) and values as high as 1 mG have indeed been reported from CN Zeeman observations of molecular clouds (Falgarone et al. 2008). Magnetic field strengths in dark clouds have only been measured towards a limited number of sources (see e.g. Troland & Crutcher 2008), where typical field strengths are estimated to be less than 30 μG .

1.3 Excitation and de-excitation

General references:

Stahler & Palla (2005); Tielens (2005)

The interstellar gas can be heated and cooled in several different ways. One important heating source is cosmic rays (mostly high velocity protons) that interact with the gas in the ISM. Cosmic rays can excite molecular hydrogen but they can also ionise atoms and molecules. This ionisation process can in turn trigger the formation of molecules. Other important heating sources are X-rays and ultraviolet (UV) radiation from the stars. The UV radiation field is generally too weak to ionise the hydrogen and helium but is strong enough to ionise some of the heavier elements. UV radiation can also release electrons from the grains and increase the temperature of the grains. X-rays are capable of ionising the atomic part of the gas, especially hydrogen and helium.

Of special interest in star-forming regions are the large-scale motions of the gas. When clouds collapse through gravitation, this compression will heat the gas. For that reason, cooling processes are important in order to allow for the final collapse and for stars to form. Molecules are more efficient than atoms in cooling the gas due to the fact that rotational transitions require much less energy than atomic transitions. The total energy of a molecule is determined by the electronic, rotational and vibrational energies. Of those, the transitions between different rotational states are the ones that involve least energy and for that reason those are most important in the cold environments of interstellar clouds. Vibrational and electronic transitions can of course be of great importance in hotter environments, but in this thesis we focus on the rotational transitions of molecules. For example, the temperatures in star forming regions are in most cases so low that only the lowest rotational levels are populated.

1.3.1 Rotational transitions

For a rigidly rotating, diatomic or linear polyatomic molecule, the kinetic energy can be described by

$$E_{\text{rot}} = B_e h J(J + 1), \quad (1.1)$$

where h is Planck's constant and J is the rotational quantum number. B_e is the rotational constant,

$$B_e = \frac{h}{8\pi^2 I}, \quad (1.2)$$

in units of frequency and I is the moment of inertia. The allowed radiative rotational transitions are for $\Delta J = \pm 1$ and the spectral lines are separated by equal $\Delta\nu$. The moment of inertia is larger for molecules with heavy atoms than for smaller molecules. Thus, it is obvious from Eq. 1.1 why the energy levels are less separated for CO than for H₂.

For non-linear molecules the description of the rotational energy is slightly more complicated. In the case of symmetric top molecules (such as NH₃), it is relatively

straightforward to describe the energy levels since two of the moments of inertia are equal. In this case, the energy levels are described by two quantum numbers, J (total angular momentum) and K (angular momentum along the symmetry axis). However, for H_2O which is an asymmetric top molecule, all moments of inertia are different. For this molecule, the rotational energy levels are described by three quantum numbers.

Carbon monoxide (CO)

CO is a diatomic molecule with a weak permanent dipole moment. Therefore, radiative transitions can occur and J is allowed to change by ± 1 . The energy levels are closely spaced and are observed at a wavelength of a few millimetres (for the low- J transitions). In molecular clouds, CO is usually excited through collisions with H_2 molecules. Since densities are often high enough, the CO molecules are found in Local Thermodynamic Equilibrium (LTE) and thus, the excitation temperature, T_{ex} is equal to the kinetic temperature, T_{kin} . This will be further discussed in Sec. 1.5.1.

Molecular hydrogen (H_2)

H_2 is a homonuclear molecule and does not have a permanent dipole moment. This means that apart from having widely separated energy levels there are no strong allowed radiative transitions that can occur. Instead, H_2 decay through weak quadrupole transitions, and transitions with $\Delta J = \pm 2$ are allowed. The even states are for the situation where the nuclear spins of the two hydrogen atoms are anti-parallel (*para*) and the odd states are for when the nuclear spins are parallel (*ortho*). The lowest allowed transition is for *para*- H_2 , from $J = 2$ to $J = 0$ in the $\nu = 0$ vibrational state (often denoted as the $0 - 0$ S(0) line), and emits photons at a wavelength of $28.2 \mu\text{m}$. The atmospheric background is very high at this wavelength and the transition is best observed with space-based telescopes. Similarly to CO, collisional excitation dominates in dense clouds so that LTE is a useful assumption to adopt (see Sec. 1.5.1).

Water (H_2O)

The H_2O molecule is an asymmetric top and the energy depends on the rotational quantum number and three rotational constants, A, B and C, which describe the orthogonal rotational axes (see Fig. 1.1). The rotational states are labelled J_{K_{-1}, K_1} where K_{-1} denotes the change of B towards C while K_1 denotes the change of A towards C. The rotational quantum number J can change by 0, +1 or -1 while K_{-1} and K_1 can change by ± 1 and ± 3 . As for H_2 , the nuclear spins of the two hydrogen atoms can be parallel (*ortho*- H_2O) or anti-parallel (*para*- H_2O). Furthermore, the quantum selection rules allow even and odd K_{-1} and K_1 to change to odd and even or vice versa. Even and even numbers can only change to odd and odd numbers and vice versa. For H_2O , it is usually not correct to assume that collisions dominate over radiative excitation and the LTE approach becomes invalid. Thus, more advanced methods for dealing with the radiative transfer are required (see Sec. 1.5.2). The lowest rotational levels of H_2O

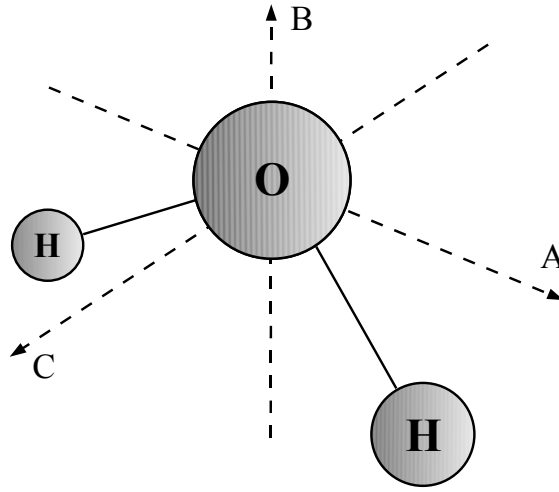


Figure 1.1: Structure of the water molecule showing the orthogonal rotational axes, A, B and C.

are shown in Fig. 1.2. In this figure, the transitions discussed in the appended papers are marked. Several of these transitions are between the different backbone states, i.e., where the fastest transitions occur. However, there are also other allowed transitions that are not discussed in the appended papers, such as the ones where the molecule leave the rotational backbone (see e.g. Neufeld & Melnick 1991). One such transition is the $6_{16} - 5_{23}$ transition at 22 GHz, where the level populations can be inverted, i.e., masing. This can in some cases pose an additional challenge for radiative transfer codes.

1.3.2 Rotational transition strength

If we consider two levels of a simple molecule such as CO, the excitation from the lower to the upper level can occur through collisions or through radiation. The probability for excitation through radiation is governed by the Einstein coefficient for stimulated absorption, $B_{J \rightarrow J+1}$ (Einstein 1917). Transition from the upper to the lower level can also occur through collisions or radiation, but in this case two different radiative de-excitations can take place. In one case an ambient photon with appropriate frequency can stimulate the transition and this is governed by the Einstein coefficient for stimulated emission $B_{J+1 \rightarrow J}$. In the other case, a photon is emitted spontaneously and the transition is governed by the Einstein coefficient for spontaneous emission, $A_{J+1 \rightarrow J}$.

When spontaneous emission occurs from the upper state ($J + 1$) to the lower state (J), the transition probability per second is given by

$$A_{J+1 \rightarrow J} = \frac{64\pi^4}{3hc^3} \nu^3 |\mu_{J+1 \rightarrow J}|^2, \quad (1.3)$$

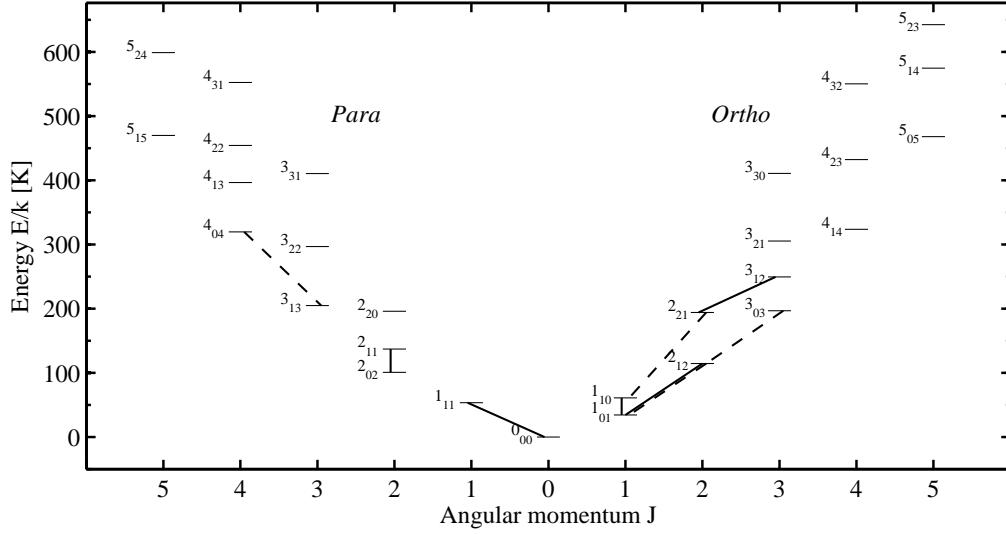


Figure 1.2: Rotational energy levels for water. The solid (HIFI) and dashed (PACS) lines indicate the transitions discussed in the appended papers.

where $\mu_{J+1 \rightarrow J}$ is the mean transition dipole moment, and ν is the frequency of the spectral line in Hz. The transition dipole moment can be expressed as

$$|\mu_{J+1 \rightarrow J}|^2 = \mu^2 \frac{J+1}{2J+3}, \quad (1.4)$$

where μ is the permanent electric dipole moment of a linear molecule. The Einstein A -coefficient for spontaneous emission is related to the Einstein B -coefficient for stimulated emission through

$$A_{J+1 \rightarrow J} = \frac{2h\nu^3}{c^2} B_{J+1 \rightarrow J}. \quad (1.5)$$

The B -coefficient for stimulated emission is related to the B -coefficient for stimulated absorption through

$$B_{J+1 \rightarrow J} = \frac{g_J}{g_{J+1}} B_{J \rightarrow J+1}, \quad (1.6)$$

where g_{J+1} and g_J are the statistical weights for the upper and lower states respectively. If the level populations (n_{J+1} and n_J) in a two-level system are constant over time then the following relationship must hold,

$$C_{J \rightarrow J+1} n_J + B_{J \rightarrow J+1} \bar{J} n_J = C_{J+1 \rightarrow J} n_{J+1} + B_{J+1 \rightarrow J} \bar{J} n_{J+1} + A_{J+1 \rightarrow J} n_{J+1}. \quad (1.7)$$

Here, \bar{J} is the mean integrated intensity, and $C_{J \rightarrow J+1}$ and $C_{J+1 \rightarrow J}$ are the collision rates per second for upward and downward transitions, respectively. The two-level system will be discussed further in Section 1.4.2.

1.4 Radiative transfer

General references:

Mihalas (1978); Rybicki & Lightman (1979)

The excitation and de-excitation of molecules and atoms is dependent on the physical conditions in the region where these processes take place. To derive properties such as temperature, density and abundance from the observed radiation one has to account for the transfer of radiation. In this section the most basic concepts of radiative transfer will be discussed.

Molecules and atoms emit radiation at specific wavelengths depending on the quantum states in which they can exist. The intensity of this radiation is independent of distance as long as radiation is not absorbed or re-emitted (or if space itself is changed). The frequency of the emitted radiation is determined by the transition between different energy levels of the molecule or atom in question. The intensity caused by a transition with frequency ν is defined as

$$I_\nu = \frac{\Delta P}{\Delta\nu\Delta A\Delta\Omega}, \quad (1.8)$$

where ΔP is the energy per unit time, $\Delta\nu$ is the frequency range of the radiation that propagates with a 90 degree angle towards the area ΔA within the solid angle $\Delta\Omega$. Although it is most convenient to use intensities when dealing with the radiative transfer, it should be noted that it is also common to express the radiation in terms of flux density, i.e., the intensity integrated over the solid angle of the source

$$F_\nu = \int I_\nu d\Omega. \quad (1.9)$$

Note that it is here assumed that the radiation propagates normal to the surface ΔA . The flux density is in contrast to the intensity dependent on the distance to the source.

1.4.1 The radiative transfer equation

The intensity change of radiation caused by a transition $l \rightarrow l'$, propagating through a slab of thickness s in a medium at steady state is governed by the equation

$$\frac{dI_{ll'}(\nu)}{ds} + \alpha_{ll'}(\nu)I_{ll'}(\nu) = j_{ll'}(\nu), \quad (1.10)$$

where $j_{ll'}(\nu)$ is the emission coefficient

$$j_{ll'}(\nu) = \frac{h\nu}{4\pi}n_l A_{ll'}\phi_{ll'}(\nu) \quad (1.11)$$

and $\alpha_{ll'}(\nu)$ is the absorption coefficient

$$\alpha_{ll'}(\nu) = \frac{h\nu}{4\pi}(n_{l'}B_{l'l} - n_l B_{ll'})\phi_{ll'}(\nu). \quad (1.12)$$

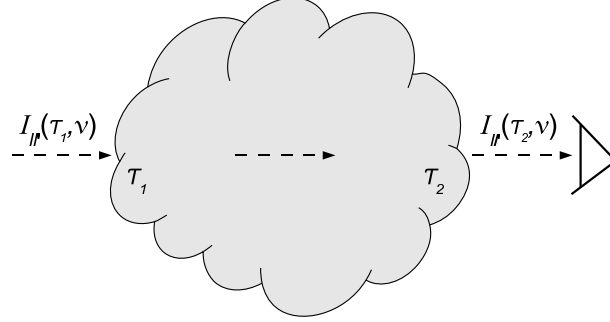


Figure 1.3: Propagation of radiation through a gas cloud.

$\phi_{ll}(\nu)$ is the normalised line profile, n_l and $n_{l'}$ are the level populations. A_{ll} , B_{ll} and $B_{l'l}$ are the Einstein coefficients for spontaneous emission, stimulated emission and stimulated absorption. The source function $S_{ll}(\nu)$ can now be defined as

$$S_{ll}(\nu) = \frac{j_{ll}(\nu)}{\alpha_{ll}(\nu)} = \frac{n_l A_{ll}}{n_{l'} B_{l'l} - n_l B_{ll}}. \quad (1.13)$$

The dimensionless optical depth along a distance ds is defined as

$$d\tau_{ll}(\nu) = \alpha_{ll}(\nu) ds. \quad (1.14)$$

If the system is emitting thermally at the temperature T , we have: $S_{ll}(\nu) = B(\nu, T)$, where $B(\nu, T)$ is the Planck function. The linear differential equation 1.10 can be written in terms of the optical depth into the cloud as

$$\frac{dI_{ll}(\nu)}{d\tau_{ll}(\nu)} + I_{ll}(\nu) = S_{ll}(\nu). \quad (1.15)$$

The integrating factor ($\exp[\tau_{ll}(\nu)]$) can easily be found, so that

$$\frac{d(I_{ll}(\nu) \exp[\tau_{ll}(\nu)])}{d\tau_{ll}} = S_{ll}(\nu) \exp[\tau_{ll}(\nu)]. \quad (1.16)$$

This can be integrated from τ_1 to τ_2 , and after division by ($\exp[\tau_2]$) we obtain

$$I_{ll}(\tau_2, \nu) = I_{ll}(\tau_1, \nu) \exp[\tau_1 - \tau_2] + \exp[-\tau_2] \int_{\tau_1}^{\tau_2} S_{ll}(\nu) \exp[\tau_{ll}(\nu)] d\tau_{ll}(\nu), \quad (1.17)$$

where $I_{ll}(\tau_1, \nu)$ is the contribution from the background. Rewriting this, we have the formal solution of the radiative transfer equation

$$I_{ll}(\tau_2, \nu) = I_{ll}(\tau_1, \nu) \exp[-(\tau_2 - \tau_1)] + \int_{\tau_1}^{\tau_2} S_{ll}(\tau', \nu) \exp[-(\tau_{ll} - \tau'_{ll})] d\tau'_{ll}. \quad (1.18)$$

This relation can be simplified if we integrate equation 1.16 from 0 to τ and assume a constant source function S and a homogeneous cloud,

$$\begin{aligned} I_{ll'}(\nu) \exp[\tau_{ll'}(\nu)] \Big|_0^\tau &= S_{ll'}(\nu) \int_0^\tau \exp[-\tau_{ll'}(\nu)] d\tau_{ll'}(\nu) \\ \Rightarrow I_{ll'}(\tau, \nu) &= I_{ll'}(0, \nu) \exp[-\tau] + S_{ll'}(\nu) (1 - \exp[-\tau]). \end{aligned} \quad (1.19)$$

The ratio between the level populations n_l and $n_{l'}$ can be defined by the excitation temperature T_{ex} ,

$$\frac{n_l}{n_{l'}} = \frac{g_l}{g_{l'}} \exp\left[-\frac{h\nu}{kT_{\text{ex}}}\right], \quad (1.20)$$

where g_l is the statistical weight of level l and $g_{l'}$ is the statistical weight of level l' . Using Eqs. 1.5, 1.6 and 1.13, we can now express the source function as

$$S_{ll'}(\nu) = \frac{2h\nu^3}{c^2} \frac{1}{\exp\left[\frac{h\nu}{kT_{\text{ex}}}\right] - 1} = B(\nu, T_{\text{ex}}), \quad (1.21)$$

where $B(\nu)$ is the blackbody radiation field at the temperature T_{ex} . Equation 1.19 can thus be written as

$$I_{ll'}(\tau, \nu) = I_{ll'}(0, \nu)e^{-\tau} + B(\nu, T_{\text{ex}}) (1 - e^{-\tau}). \quad (1.22)$$

In radio astronomy, it is customary to define a brightness temperature in the Rayleigh-Jeans limit (the indices l and l' have here been dropped)

$$T_{\text{B}}(\nu) = \frac{c^2}{2k\nu^2} I(\nu) \quad (1.23)$$

One can therefore rewrite Eq. 1.22 as

$$T_{\text{B}}(\nu) = T_{\text{bg}}(\nu)e^{-\tau} + T_{\text{ex}} (1 - e^{-\tau}). \quad (1.24)$$

Astronomers often use the quantity antenna temperature, T_{A} . The antenna temperature is, however, only equal to the brightness temperature when the source is much larger than the antenna beam and the antenna is completely lossless. Also, the main beam brightness temperature, T_{mb} is often used, where the main beam efficiency has been taken into account (and the attenuation of the atmosphere for ground-based telescopes).

In a molecular cloud, the excitation in each position is affected by emission originating in all other parts of the cloud. It is therefore useful to define the mean integrated intensity averaged over all directions μ

$$\bar{J}_{ll'} = \frac{1}{4\pi} \int d\Omega \int d\nu \phi_{ll'}(\mu, \nu) I_{ll'}(\mu, \nu). \quad (1.25)$$

1.4.2 Statistical equilibrium

If the level populations are defined, the intensity can be calculated using equation 1.17. The issue when dealing with these problems is the fact that the level populations are not that easily determined. The statistical equilibrium equations (SE) are:

$$\begin{aligned} & \sum_{l' < l} [n_l A_{ll'} - (n_{l'} B_{l'l} - n_l B_{ll'}) \bar{J}_{ll'}] - \\ & \sum_{l' > l} [n_{l'} A_{l'l} - (n_l B_{ll'} - n_{l'} B_{l'l}) \bar{J}_{ll'}] + \\ & \sum_{l'} (n_l C_{ll'} - n_{l'} C_{l'l}) = 0, \end{aligned} \quad (1.26)$$

where $C_{ll'}$ and $C_{l'l}$ are the collision rates per second. These rates are related to the collision rate coefficients, $R_{ll'}$ (in $\text{cm}^3 \text{s}^{-1}$), as

$$C_{ll'} = R_{ll'} n_{\text{coll}}, \quad (1.27)$$

where n_{coll} is the density of the collision partner. In star forming regions, it is in most cases a good approximation to assume that all collision partners are H_2 molecules. A simple case is when the density is so high that collisional transitions totally dominate. In this two-level system (with energy levels $E_u > E_l$), we have LTE ($T_{\text{ex}} \rightarrow T_{\text{kin}}$) and the level populations follow the Boltzmann distribution

$$\frac{n_u}{n_l} = \frac{C_{lu}}{C_{ul}} = \frac{g_u}{g_l} \exp \left[\frac{-(E_u - E_l)}{kT_{\text{kin}}} \right]. \quad (1.28)$$

The SE equations can in the two-level system be expressed in a simpler form

$$\begin{aligned} \frac{dn_l}{dt} &= -n_l(B_{lu}\bar{J} + C_{lu}) + n_u(A_{ul} + B_{ul}\bar{J} + C_{ul}) = 0 \\ \frac{dn_u}{dt} &= +n_l(B_{lu}\bar{J} + C_{lu}) - n_u(A_{ul} + B_{ul}\bar{J} + C_{ul}) = 0. \end{aligned} \quad (1.29)$$

The density, when downward radiative processes equal the downward collisional processes, is called the critical density

$$n_{\text{crit}} = \frac{A_{ul} + B_{ul}\bar{J}}{R_{ul}}. \quad (1.30)$$

The radiation field can often be neglected and the relation $n_{\text{crit}} = A_{ul}/R_{ul}$ is frequently used.

1.5 Radiative transfer analysis

An important step in interpreting the spectroscopic data is to compare it with models. Different methods for the radiative transfer analysis may be used dependent on

whether the molecule of interest is in LTE or out of thermal equilibrium. The first scenario is very simple in the sense that the level populations are only temperature dependent (Eq. 1.28). Therefore, the temperature and column density of the gas can be readily obtained from a population diagram analysis as long as the emission is optically thin and more than one transition is observed. In the latter scenario on the other hand, more sophisticated methods have to be used and these require knowledge of collisional data. The difficulty when solving these problems is the coupling between the radiation field and the level populations (Eqs. 1.13, 1.19, 1.25 & 1.26). This section provides a discussion of the different methods that can be used for the analysis of molecular line data.

1.5.1 Thermal equilibrium

A molecule is said to be in LTE when the excitation and de-excitation of the rotational levels are dominated by collisions, i.e., the density is much higher than the critical density, n_{crit} (Eq. 1.30). This particularly simple scenario is often valid for the pure rotational transitions of H_2 in the first vibrational state. For example, for the H_2 0–0 S(0) line, the critical density is always lower than 10^2 cm^{-3} . If several transitions of the rotational ladder are observed, population diagram analysis may be used (see e.g. Linke et al. 1979; Goldsmith & Langer 1999). For optically thin emission, the column density of the upper state is given by

$$N_u = \frac{8\pi k\nu^2}{hc^3 A_{ul}} \int T_{\text{mb}} dv, \quad (1.31)$$

where the quantities have their usual meaning. In LTE, the excitation temperature is equal for all the rotational levels and the population of each state follow the Boltzmann distribution

$$N_u = \frac{N}{Z} g_u e^{-E_u/kT}, \quad (1.32)$$

where N is the total column density and Z is the partition function. Eq. 1.32 can also be expressed as

$$\ln \frac{N_u}{g_u} = \ln \frac{N}{Z} - \frac{E_u}{kT}. \quad (1.33)$$

The column density and the rotational temperature (in this particular case the kinetic temperature) of the gas can now readily be obtained by fitting a straight line to the observed values. This method is used in Paper III, to investigate the temperature and spatial distribution of H_2 . However, in the dense regions, where outflows are located, extinction effects may be important also in the infrared range (see e.g. Rieke & Lebofsky 1985). The extinction at a certain wavelength is related to the ratio between the observed and actual flux by

$$A_\lambda = -2.5 \times \log_{10} \left(\frac{F_{\text{obs}}}{F} \right). \quad (1.34)$$

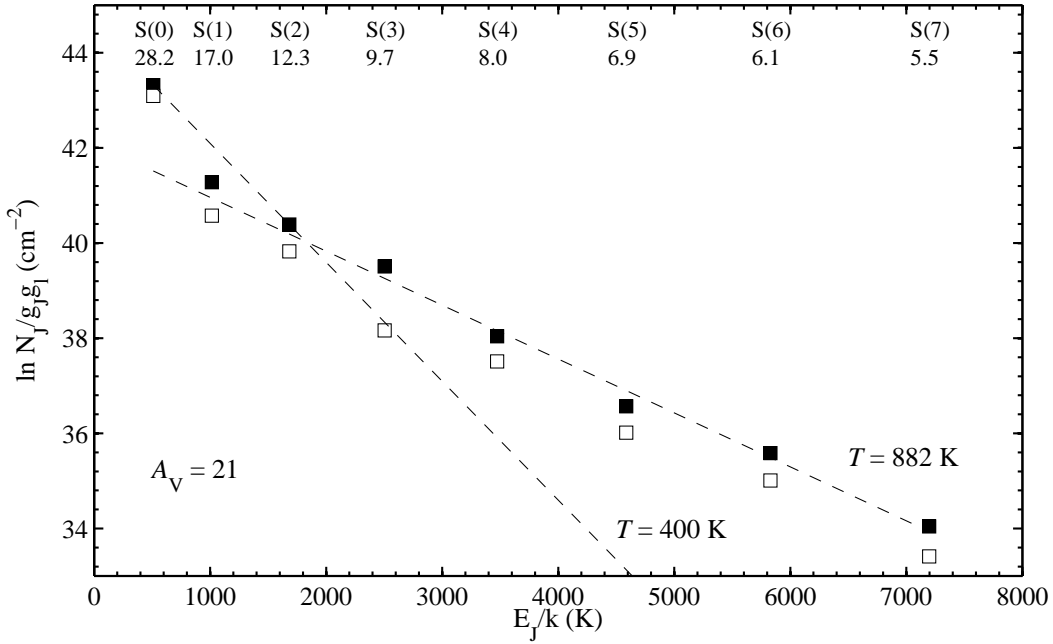


Figure 1.4: Population diagram of H₂ towards the B1 position in VLA 1623 showing the observed values (open squares) and those that have been corrected for extinction (filled squares). The visual extinction was taken to be $A_V = 21$ (Liseau & Justtanont 2009, Paper III). The vertical axis shows the natural logarithm of the upper state column density divided by the product of the statistical weights associated with rotation and spin. The horizontal axis shows the upper state energies divided by Boltzmann's constant. Labels and wavelengths (in μm) are given above the graph. The diagram shows the presence of two temperature components at ~ 400 K and ~ 900 K respectively. Also the effect of the silicate feature at $10 \mu\text{m}$ on the S(3) line is evident from this figure.

If the extinction at each wavelength is known, the actual flux at each wavelength can be obtained from

$$F = F_{\text{obs}} \times 10^{0.4 \cdot A_\lambda}. \quad (1.35)$$

Deriving the extinction curve can be a difficult task, but for the purpose of this thesis, the curve derived by Rieke & Lebofsky (1985) is sufficient to use. An example of an extinction corrected population diagram is shown in Fig. 1.4.

1.5.2 Non-thermal equilibrium

So far, LTE has been discussed, but this situation is certainly not always the case. In contrast to H₂, the H₂O molecule is rarely in LTE due to the relatively large critical densities. For systems of this type one must instead rely on more complicated procedures. As described by van der Tak et al. (2007), these methods can be split into intermedi-

ate and advanced methods. One such intermediate method is the one used by RADEX³, where an assumption of a homogeneous medium is used to limit the numbers of free parameters. Examples of advanced methods are Accelerated Lambda Iteration (ALI, Rybicki & Hummer 1991) to calculate the intensity as a function of velocity and depth into the cloud, or to use Monte Carlo techniques. The advantage of the latter ones is that the problem is solved exactly (for the adopted discrete geometry) but at the cost of computing power. These techniques also allow for choosing arbitrary temperature, density and velocity structures as well as complicated source geometries. The use of RADEX is simple and fast. In the work presented in this thesis, all these different methods have been used.

Escape probability method

The computer program RADEX uses the method of escape probability for the radiative transfer. It was originally written by John H. Black and is described in detail by van der Tak et al. (2007). The problem of the coupling between the radiation field and the level populations is solved by introducing an escape probability, β , or the chance for a photon to escape the cloud (dependent on the optical depth of the cloud). This quantity is related to the intensity as

$$\bar{J} = S(1 - \beta), \quad (1.36)$$

i.e., the radiation field is decoupled from the solution of the level populations. In RADEX, three different expressions for the escape probability can be used (i.e., different source geometries). These are, expanding homogenous shell (LVG), homogenous sphere and plane-parallel slab.

Accelerated Lambda Iteration (ALI)

The non-LTE code ALI, developed by Per Bergman (Justtanont et al. 2005; Maercker et al. 2008; Wirström et al. 2010), uses the Accelerated Lambda Iteration technique to solve the radiative transfer problem exactly in a spherically symmetric geometry. An initial guess of the level populations, n_i , is made and the statistical equilibrium equations (1.26) are solved by first calculating the mean integrated intensity at every radial position in the sphere. Taking the direction of the radiation into account as well as the dust, the specific intensity can be obtained from the relation

$$I(\mu, \nu) = I_{\text{bg}}(\mu, \nu)e^{-\tau_{\text{tot}}(\mu, \nu)} + \int_0^{\tau_{\text{tot}}(\mu, \nu)} S_{\text{tot}}(\mu, \nu)e^{-\tau_{\text{tot}}(\mu, \nu) + \tau'} d\tau, \quad (1.37)$$

where the first term is the contribution from the background and S_{tot} is the total source function including dust (and overlapping lines). The mean integrated intensity can then be obtained from Eq. 1.25 by integrating the specific intensity over all directions and frequencies. Using the calculated mean integrated intensity, new level populations

³<http://www.sron.rug.nl/~vdtak/radex/>

can be calculated from the statistical equilibrium equations (Eq. 1.26). The new level populations are used in Eq. 1.37 and the procedure is continued in an iterative manner until convergence is reached. In the ALI code, the specific intensity is obtained after introducing the lambda operator $\Lambda(\mu, \nu)$ and Eq. 1.37 can be rewritten as

$$I(\mu, \nu) = \Lambda(\mu, \nu) [S_{\text{tot}}(\mu, \nu)] + I_{\text{bg}}(\mu, \nu) e^{-\tau_{\text{tot}}(\mu, \nu)}. \quad (1.38)$$

The lambda operator can be interpreted as a matrix of size $N \times N$ with N radial points. The local contribution to the mean integrated intensity is in the diagonal elements while the non-local contributions are described in the off-diagonal elements. The advantage of the Accelerated Lambda Iteration technique compared to the Lambda Iteration technique is that it takes care of the high optical depths separately. This is accomplished mathematically through an operator splitting technique that introduces an approximate lambda operator.

Collision rates

As already mentioned, the use of radiative transfer codes like RADEX or ALI, requires knowledge of the collisional rate coefficients. In recent years, considerable efforts have been put into calculating new rate coefficients for collisions between H_2O and H_2 . For this reason, different sets of collision rates have been used in the different papers appended to this thesis. These data files have been downloaded from the LAMDA⁴ database (Schöier et al. 2005). The most recent collisional rate coefficients for collisions with *p*- H_2O and *o*- H_2O (Dubernet et al. 2006, 2009; Daniel et al. 2010, 2011) were used in Paper III, however, an older set (Faure et al. 2007), where the rate coefficients can differ by up to a factor of 3 compared to the newer ones, was used in Paper I. In Fig. 1.5, the RADEX results for a few transitions (when using different sets of collisional rate coefficients) are compared. The results are computed for a range of H_2 densities ($10^5 - 10^6 \text{ cm}^{-3}$) and H_2O column densities ($10^{13} - 10^{15} \text{ cm}^{-2}$), having a fixed line width of $\Delta\nu = 20 \text{ km s}^{-1}$. For these transitions, the results are typically within a factor of 2 when using the different sets of collisional rate coefficients. Note that for programs like RADEX, the optical depths (and therefore the computed line intensities) are dependent on the LVG parameter, $N/\Delta\nu$.

⁴<http://www.strw.leidenuniv.nl/~moldata>

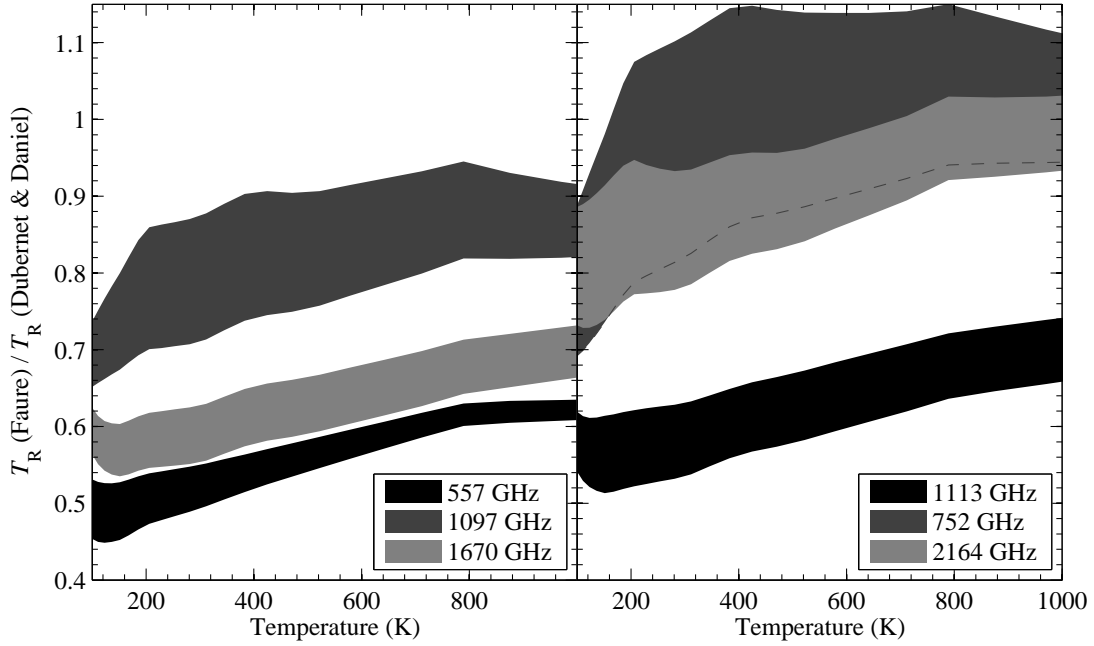


Figure 1.5: Comparison between the different sets of collisional rate coefficients used in the appended papers. The coloured regions represent line strength ratios computed with RADEX when $n(\text{H}_2) = 10^5 - 10^6 \text{ cm}^{-3}$, $N(o,p\text{-H}_2\text{O}) = 10^{13} - 10^{15} \text{ cm}^{-2}$ and $T = 100 - 1000 \text{ K}$. In this case the line width is set to be constant, i.e., $\Delta v = 20 \text{ km s}^{-1}$. The overlap between the 2164 & 752 GHz regions is indicated with a dashed line.

Chapter 2

Low-mass star formation

General references: Masunaga & Inutsuka (2000); Stahler & Palla (2005)

As noted in Chapter 1, star formation is an ongoing process and it will continue for a long time to come. Stars are part of the recycling process that is continuously active in the Galaxy and they are formed when dense regions of interstellar clouds collapse. During their lifetime they undergo mass-loss to various extent and therefore interstellar matter can be recycled several times. The observations discussed in this thesis are focused on low-mass objects but it should be noted that high-mass stars are important sources for the injection of heavier elements into the ISM through super-nova explosions.

The star formation process involves several different evolutionary stages, starting with the fragmentation of molecular clouds and ending with a newly born star (see e.g. Shu et al. 1987). In the last few decades, significant progress has been made in order to understand this process, and it has become a field in astronomy of extensive research, not the least through the use of facilities like *Herschel* and ALMA. Reviews of the progress in this research field over the years have been presented in the “Protostars and planets” series (see e.g. Mannings et al. 2000; Reipurth et al. 2007).

2.1 Gravitational collapse

Stars that are much younger than the Galaxy are observed frequently, but this does not mean that stars are formed everywhere all the time. The star formation rate can indeed be very high on comparatively short time scales, e.g., due to collisions between galaxies, but the fact that widespread interstellar gas is observed suggests that this type of phenomena is transient. Thus, the greatest proportion of interstellar gas must be able to withstand gravitational forces by means of thermal pressure, turbulence, rotation and the support of large-scale magnetic fields. And conversely, it is these opposing forces that have to be overcome in order to allow for the gravitational force to increase

the gas density by some 20 orders of magnitude.

Assuming that only thermal pressure and gravity affect a dense core, this core can collapse and eventually form a stellar system if the mass is larger than the Jeans mass

$$M_J \simeq \frac{c_s^3}{\rho^{1/2} G^{3/2}}, \quad (2.1)$$

where ρ is the density, G is the gravitational constant. The speed of sound c_s is proportional to the square root of the temperature. Therefore, it is obvious that the gas must be relatively cold in order for a dense core to undergo collapse. This is clearly illustrated if Eq. 2.1 instead is written as

$$M_J \simeq 2M_\odot \left[\frac{T}{10 \text{ K}} \right]^{3/2} \left[\frac{n(\text{H}_2)}{10^5 \text{ cm}^{-3}} \right]^{-1/2}. \quad (2.2)$$

As the contraction goes on it is reasonable to assume that some part of the gravitational energy can be converted to heat and the core should therefore be warmed up. Therefore, efficient cooling processes are important in these regions. From Equation 2.1, one can also conclude that when the density increases during collapse, the critical mass will decrease (as long as the sound speed does not increase). It is therefore likely that the collapse breaks up into fragments and this is also consistent with the observation that most stars form in groups (see e.g. Lada & Lada 2003). If other forces that counteract gravity are present (which is most likely the case), the critical mass can be significantly higher than the value that is derived from Equation 2.2.

A dense core that is stable against gravitational collapse can become unstable when an external pressure is applied to the cloud. When this leads to the formation of one or several stars, it is usually referred to as triggered star formation or induced star formation. The cause of these pressure increases may for example be adjacent supernova explosions, cloud-cloud collisions or outflow activity. Therefore, star formation can be a sequential phenomenon where forming stars triggers the formation of other stars.

Equation 2.1 is in most cases a severe simplification of the reality due to the presence of other forces. For example, it is extremely unlikely that no initial rotation is present and the support from magnetic fields has so far been ignored. Any initial rotation will increase during the collapse and this will result in a twisted magnetic field that increases the magnetic tension. This will act as a breaking torque, decreasing the specific angular momentum. However, close to the centre, the density is so high that this theory breaks down. Inside some radii, the specific angular momentum will be conserved. In this region a particle can end up either in the disk, the outflow or it falls onto the forming protostar.

2.2 Protostellar formation

Turning our attention to the inner region, the formation of the protostar occurs in a stepwise manner highly dependent on the temperature (see e.g. Masunaga & Inutsuka

2000; Stahler et al. 1980). When contraction goes in to the final stages, temperatures are increasing significantly. The reason for this is that the central region becomes opaque to infrared radiation, preventing escape of the photons. As material is falling onto the inner core, it will slowly start to contract. When the core becomes smaller, the mass will increase due to infalling material and the temperature will increase. At some point the H_2 molecules start to dissociate and this initially has the effect of stabilising the temperature of the core and slowing down the contraction speed. However, the damping of the contraction can only continue up to a certain point and the core finally collapses under its own gravity. Now, the temperature starts to increase again and most of the hydrogen is ionised. This allows the newborn protostar to stay dynamically stable and it is at this time in protostellar evolution when the protostar enters the so-called main accretion phase. During this phase, most of the luminosity is due to accretion of material onto the protostar and the circumstellar disk (depending on rotation). The accretion continues until the temperature becomes high enough, allowing the protostar to ignite deuterium. This is the first fusion process that occurs and the temperature when this happens is around 10^6 K. The deuterium burning increases the luminosity so much that radiation cannot transport away all of the energy. For this reason convection processes also begin. The deuterium burning has the effect of increasing the radius, however, the amount of expansion is highly dependent on the accretion rate.

In rotating systems, material first goes into the disk surrounding the protostar. This means that the mass of the protostar can grow in two ways. Either the infall rate increases or the rotation speed of the protostar decreases. Due to the centrifugal forces, the first scenario is not realistic. It is reasonable to assume that the protostar must suffer some kind of braking torque, and this is where the stellar wind comes into the picture.

The star formation process implies that several components should be present in the vicinity of young stellar objects (YSO's). The protostellar envelope and the parental cloud surrounds the inner region, where the first component contains gas and dust that can accrete on to the central object. As a consequence of angular momentum conservation, a disk is present closest to the stellar object. This is the site where planets eventually can form but it is also close to this region where outflows are ejected (see Chapter 3). The different stages of the star formation process (from the fragmentation of molecular clouds to T Tauri stars¹) are illustrated in Fig. 2.1.

2.2.1 Classification of young stellar objects

Due to the presence of grains in the circumstellar region, YSO's will exhibit infrared excess. A classification scheme, which is to some extent related to the age of the objects, is therefore often used. YSO's are generally divided into several subcategories dependent

¹T Tauri stars are young variable objects named after the star T Tauri in the constellation Taurus. They have masses comparable to the mass of the Sun and represent the intermediate evolutionary stage between protostars and evolved low-mass stars.

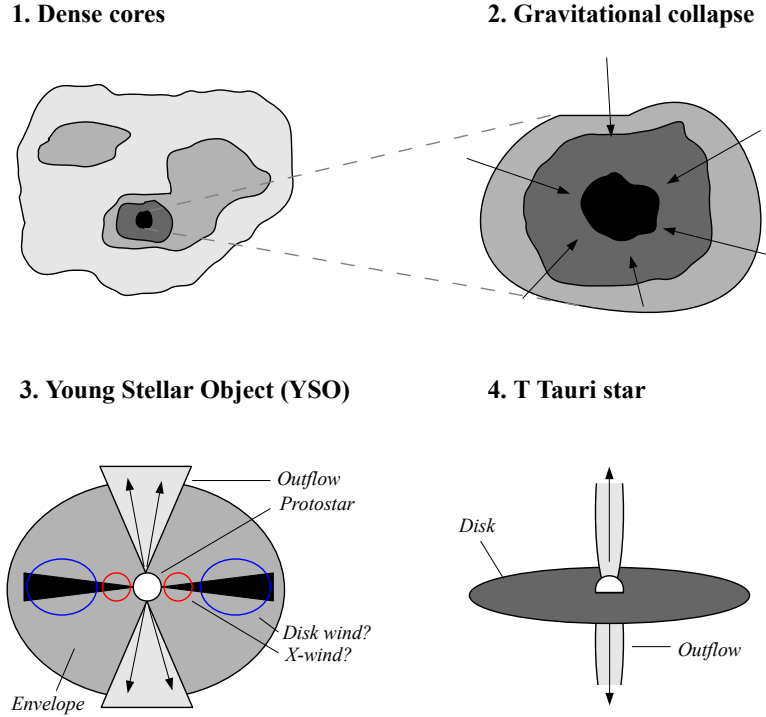


Figure 2.1: Cartoon image illustrating the different stages in the star formation process, from pre-stellar cores to T-Tauri stars.

on the observed spectral energy distribution in the infrared regime,

$$\alpha_{\text{IR}} = \frac{d \log(\lambda F_{\lambda})}{d \log \lambda}. \quad (2.3)$$

Initially three classes were defined by (Lada 1987), i.e., Class I, Class II and Class III. It turned out later, however, that the emission from some sources couldn't be classified according to this scheme. Greene et al. (1994) added the so called "Flat Spectrum" class and the discovery of VLA 1623 led to the addition of another class indicative of very young objects, i.e., Class 0 (André et al. 1993). This type of sources shows strong sub-millimetre emission but virtually no emission is detected at shorter wavelengths. The five classes, with the limits used by Greene et al. (1994), are:

- Class 0, not detectable in the near-IR regime
- Class I, $\alpha_{\text{IR}} > 0.3$
- Flat Spectrum, $-0.3 < \alpha_{\text{IR}} < 0.3$
- Class II, $-1.6 < \alpha_{\text{IR}} < -0.3$
- Class III, $\alpha_{\text{IR}} < -1.6$

The Class 0 and Class I type sources are generally considered to be very young (Lada 1987), but it should be noted that it is difficult to consolidate a certain class with an evolutionary stage (see e.g. Crapsi et al. 2008).

2.3 Observing the star formation process

Newly born stars are extremely difficult to observe directly, since the surrounding dust effectively absorbs and/or re-emits all radiation originating from the central object. YSO's can therefore not be observed in the visible regime. Instead, radiation that can be detected at longer wavelengths has proven to be an important probe for these very young systems. Class I sources can be readily observed through the dust emission in the infrared. The dust surrounding Class 0 sources is, on the other hand, not detected shortward of 10 μm and here one has to observe at even longer wavelengths to find them. From the observational evidence it is clear that a relatively larger amount of dust is present in the vicinity of Class 0 sources than the more evolved Class I sources (André & Montmerle 1994).

A well-known property of Class 0 sources is that they are associated with highly collimated outflows that move at high velocities. One can therefore conclude that these objects reside in energetic environments. The number of known Class 0 sources is, also, still quite small and this suggests that this phase constitutes a relatively short time in the star formation process. However, to clearly identify these objects as protostars, one would have to observe one of the most fundamental processes in star formation, namely the infall of matter. Observations of a special type of self-absorbed, optically thick lines can be a sign of infall. For a collapsing spherical geometry, where the density and temperature increase towards the centre, it will be more likely for blue-shifted than for red-shifted photons to escape the cloud. Therefore, one would expect to observe a line profile where the blue-shifted component is enhanced with respect to the red-shifted one. Using different tracers, it has indeed been shown that this type of profile is more frequently observed towards Class 0 sources than towards Class I sources (see e.g. Mardones et al. 1997; Kristensen et al. 2012). However, caution should be adopted since several other processes that can account for the observed line profile shapes are involved. Infall profiles have also been observed towards star-less cores (see e.g. Tafalla et al. 1998) that are clearly not in the protostellar phase. All in all, the most prominent feature associated with the formation of stellar systems is in fact outflows.

Chapter 3

Molecular outflows

General references:

Bachiller & Tafalla (1999); Hartigan et al. (2000); Stahler & Palla (2005); Arce et al. (2007)

When molecular outflows were first discovered, this was totally unexpected. Since stars form through gravitational collapse of dense gas, one would expect to detect gas moving inwards, towards the YSO's, not outwards. However, during the last decades it has turned out that the most prominent phenomenon associated with stellar birth is in fact outflows. These structures are not spherically symmetrical but generally in the shape of two distinct lobes varying in width, length and shape. Outflows can be observed in a wide range of wavelengths and the first hint of outflow emission was in fact observed in the optical regime more than hundred years ago. The emission nebulae that are associated with bipolar outflows were presented by Sherburne W. Burnham (Burnham 1890) but it was not until the 50's that more detailed studies were carried out by George Herbig and Guillermo Haro (Herbig 1950; Haro 1952). At that time, however, it was not recognised that the observed nebulosities (usually called Herbig-Haro objects or HH-objects) were associated with high-velocity winds interacting with the ambient cloud surrounding young stars.

Molecular gas moving at high velocities was observed already during the 70's (see e.g. Wilson et al. 1970; Zuckerman et al. 1976), but the first bipolar molecular outflow (L 1551) was discovered by Snell et al. (1979, 1980). From the CO (1–0) observations presented by these authors it was clear that the outflow is separated in two lobes where gas in one lobe is red-shifted, with respect to the velocity of the cloud, while the gas associated with the other lobe is blue-shifted. Spectrally resolved line profiles thus provide us with valuable kinematical information of the source.

It has later turned out that outflow activity is a very common phenomenon and today several hundred CO outflows from young stars at different masses have been detected (Wu et al. 2004). It seems now like most (if not all) stars undergo a stage where stellar winds are ejected and outflows are therefore closely linked to the formation of stars. It has also been shown that most outflows are bipolar (84%), but there are also



Figure 3.1: The ρ Ophiuchi A cloud core imaged with Spitzer-IRAC (3.6 to 8.0 μm). The VLA 1623 outflow (green knots) is visible to the south of the comet-like nebulae. Credit: NASA/JPL-Caltech/Harvard-Smithsonian CfA

examples of monopolar flows (Wu et al. 2004) and quadrupolar flows.

3.1 Properties of outflows from low-mass objects

The acceleration of outflows most probably takes place in a region that current telescopes are not able to resolve spatially. In contrast to these confined regions, outflows can be observed on a scale of degrees (i.e., parsecs for nearby sources). Therefore, any theory that claims to explain how outflows are accelerated must also explain a number of general properties that can be observed on a much larger scale. Since low- J CO transitions are readily observed using ground-based telescopes, this molecule has been used extensively to derive the physical properties of outflows in the past. It should be noted that these transitions predominantly trace the cold gas in the outflow. It is not until recently that the warm/hot gas successfully has been observed with space-based telescopes such as ISO and *Herschel*.

From spectroscopic observations of CO one can infer the mass of the flows assuming a certain CO/H₂ abundance ratio, but also kinematical information of the gas is

obtained in this type of observations. Therefore it is relatively straightforward to derive several other physical parameters of an outflow. In cases where the size of the outflow is known, one can readily infer the dynamical time-scale. From spectrally resolved maps it is thus possible to also determine parameters such as momentum, momentum rate (force), kinetic energy and the mechanical luminosity (power) of the flow. The uncertainty, when estimating these parameters, can on the other hand be high. Not the least, the inclination angle of the flow is a contributing factor but also the bow shaped structure of the jet-flows is important in this regard (Downes & Cabrit 2007). These uncertainties are discussed in more detail in Paper III and IV but nevertheless, from the work that has been presented in the literature over the years, it is clear that the mass, momentum rate and mechanical luminosity is correlated with the bolometric luminosity of the central object (Cabrit & Bertout 1992).

The momentum rate of outflows is in general orders of magnitude higher than L_{bol}/c of the central source. It is therefore reasonable to assume that the acceleration of outflows cannot be due to radiation pressure. From resolved maps of outflows it is also possible to estimate the collimation factor (length-to-width ratio). This ratio can vary dramatically between different outflows but there seems to be a trend that the highest collimation is found in the outflows emanating from the youngest sources (Bachiller & Tafalla 1999). One example of such a highly collimated/young outflow is VLA 1623 (André et al. 1990) discussed in Paper III.

There is also clear evidence that the bulk of the emission from CO and other molecules is due to the interaction with the ambient medium. In some outflows it appears that gas which is moving at low velocity is located in a shell-like structure which surrounds the inner regions of the flow, where the high-velocity gas is detected (see e.g. Hirano et al. 2010). The number of flows mapped at a sufficient resolution to detect this difference in spatial distribution is for natural reasons limited, but there is also another indication to that the bulk of the mass in outflows is entrained. For many outflows the mass of the swept up material is much larger than the mass of the Sun (see e.g. Snell 1987) and for some high-mass sources the total outflow mass is as high as several thousand M_{\odot} (Ridge & Moore 2001). Therefore, material must have been entrained at some point. The mass of the entrained low-velocity gas is generally higher than the mass of the high-velocity gas. Furthermore, the mass-velocity relationship follows a slope that is steeper at higher velocities than at lower velocities (Bachiller & Tafalla 1999).

Of great interest for the understanding of how outflows are accelerated is the observed spatial distribution of the gas, which moves at different velocities. For example, it has been observed that the highest velocities are found at the largest distance from the central source. This is not what one expects when outflows are accelerated in a region near the central object and this behaviour is occasionally referred to as the ‘‘Hubble-law’’ of outflows. It can be understood if the total momentum is conserved and the density decreases with increasing distance from the central object. In some sources, gas moving at very high velocities is detected (see e.g. Bachiller et al. 1990). These features, also commonly referred to as bullets, seem to be ejected in episodic events since they have been observed to be symmetrically located on each side of the source (see e.g.

Bachiller et al. 1990; Santiago-García et al. 2009). Recent observations show that the gas composition differs between the low and the very high-velocity gas. Thus, this component of the gas can give valuable insights into the conditions of the innermost regions close to the protostars (Tafalla et al. 2010).

Over the years, several processes that explain the different properties of molecular outflows have been proposed. The two most appealing solutions to how outflows are accelerated are the so-called wide-angle winds (see e.g. Shu et al. 1991) and the jet-driven winds (see e.g. Masson & Chernin 1993). These models are successful in producing the observed mass-velocity slope as well as the increasing velocity with distance from the central source.

3.1.1 Shocks

Supersonic outflows from young, low-mass and relatively nearby sources, are excellent environments for studying interstellar shock physics. The chemical composition of the outflows is strongly influenced by the type of shock present, where heating and compression of gas and dust lead to chemical processes that are otherwise not possible. The composition of the gas can be significantly altered but also refractory elements can be sputtered from the grains and injected into the gas. In this sense, outflows from Class 0 sources are of particular interest because they are more energetic than outflows from evolved sources. The regions where the highest velocities are observed are often characterised by the so-called Herbig-Haro objects.

The type of shock that will arise depends largely on the processes that drive the outflow and the structure of the surrounding medium (see e.g. Draine 1980). When a fast shock encounters the ambient cloud at supersonic velocities, no forehand information in the form of sound waves is given to the pre-shock gas. In this type of environment gas densities and temperatures raise suddenly and violently and this type of shock is usually called “J-shock” (Jump shock). However, depending on the magnetic field strength, ionisation fraction and velocity of the shock, the temperature and density increase may not occur that abrupt. For example, the ionisation fraction of the pre-shock gas can increase due to ultraviolet radiation originating in the warm post-shock region. Furthermore, it is possible for magnetic waves to traverse the shock front, thereby exciting the pre-shock ions. When these effects are important enough to cause a smooth increase in temperature and density for both the ions and the neutral species, the shock is usually called a “C-shock” (Continuous shock).

Shocked regions are often observed to have a bow-shaped structure. Clear examples of this can be found in many of the beautiful optical images taken with the Hubble Space Telescope. When fluids collide at supersonic speeds, two shocks are directed away from each other in the opposite directions. The bow-shock, located at the leading edge of the shock, accelerates the downstream material while the Mach disk (see e.g. Fridlund & Liseau 1998) slows down the upstream material. In between these shocks, the pressure increase causes material to be ejected in the transverse direction. In the purely jet-driven scenario, however, it is difficult to explain outflows with large opening

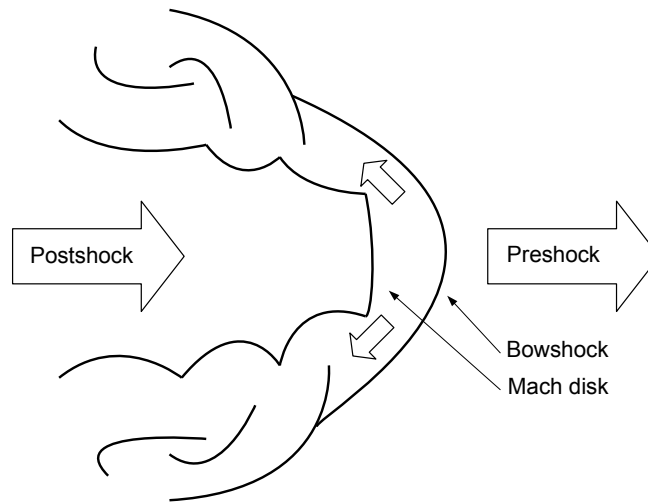


Figure 3.2: A curved shock front, created when a jet propagates into the ambient cloud. The gas is ejected in the transverse direction, as indicated with the arrows.

angles (Cabrit et al. 1997). There have been suggestions that time variability of the jet itself may circumvent this problem (Gueth et al. 1996; Lee et al. 2002) but, still, the solution to this problem is yet to be found.

3.1.2 Origin of outflows and ejection mechanisms

How outflows are accelerated is still a bit of a mystery. Although it is now believed, that outflows are directly linked to protoplanetary disks (see e.g. Cabrit et al. 1990), the exact mechanism of ejection is still a matter of debate. Accretion disks are often also observed in the vicinity of the youngest sources, known to host the most powerful outflows. One such example is VLA 1623 (Pudritz et al. 1996).

Jets seem to be a phenomenon governed by physics that operate on a wide range of scales. Analogue to jets from YSO's are the structures observed in the near vicinity of black holes of different sizes and other astronomical objects (see e.g. Livio 2004). The physics governing the redistribution of angular momentum in YSO's, therefore most likely apply also to other environments. For that reason the understanding of outflows is important also in a broader astrophysical context.

As noted already in Section 3.1, several different models have been proposed to explain the acceleration of outflows (see e.g. Arce et al. 2007). However, these models have

difficulties in explaining some of the observed features of outflows. The jet-driven wind (see e.g. Masson & Chernin 1993) models have (as mentioned earlier) difficulties in explaining the large opening angles of some outflows. The wide-angle wind (see e.g. Shu et al. 1991) models, on the other hand do not reproduce the characteristic bow-shaped structures observed in other sources. In summary, the first scenario has been most appealing for some sources while the second scenario has been in better agreement with the observations of other sources. A unified solution to the outflow acceleration problem may lie in a combination of the two processes. As noted by Shang et al. (2007), the key issue in this context may actually be at what radii the acceleration takes place. It may be near the protostar (X-wind, Shu et al. 2000), in a wide range in radius of the circumstellar disk (Disk-wind, Königl & Pudritz 2000) or a combination of the two. In any case, it is the magnetic field, the centrifugal forces and the infalling material that is responsible for the flow. In recent years, considerable efforts have been made to construct a unified model explaining jets and outflows (see e.g. Shang et al. 2006; Banerjee & Pudritz 2006; Machida et al. 2008).

3.2 Molecules in outflows

In the past, outflow emission has predominantly been traced using spectroscopic observations of the CO molecule. However, there are also other molecules of particular interest in outflow research. As mentioned already in the previous section, the chemistry of outflows is peculiar in the sense that different types of shocks have affected the gas and dust. The abundances of various species can in the presence of a shock be enhanced by order of magnitudes, why many different molecules are often observed in shocked regions (see e.g. Codella et al. 2010). One example of an outflow with such high molecular richness is the outflow emanating from the Class 0 source L 1157 and this type of outflow is often referred to as a “chemically active outflow” (Bachiller et al. 2001).

Over the last decades it has become evident that not only gas-phase reactions have to be considered in order to understand outflow chemistry. Dust evaporation, sublimation and dust surface reactions may have a profound impact on the chemistry in molecular outflows. Although many molecules have been detected in outflows to this date, this section will mainly focus on the species of particular interest for this thesis.

3.2.1 CO

Carbon monoxide was detected in space in 1970 (Wilson et al. 1970), and already in the discovery paper, signs of outflows were obvious. Since then, CO has been the most widely observed tracer of entrained outflow gas. Compared to H₂O, CO has a relatively low permanent dipole moment (0.1 Debye) and thus, it is easily excited in molecular clouds. The lowest transitions (i.e., CO (1–0), CO (2–1) and sometimes higher transitions) are therefore often seen also in the ambient gas moving at cloud velocities. One of the reasons why the lower transitions of CO have been observed so frequently is

that the emission easily can be detected with ground-based telescopes. Thus, many of the properties described in the previous section have predominantly been derived from observations of this molecule.

Some of the higher- J CO transitions were observed already with ISO (see e.g. Nisini et al. 1999) but it was not until the launch of *Herschel*, that the very high- J CO lines (up to $J = 49 - 48$ at $E_u/k = 6724$ K) were probed successfully towards outflows (Herczeg et al. 2012). These lines trace a gas component much warmer than the gas component traced by the low- J CO transitions.

3.2.2 H₂O

Interstellar water was detected from the ground already in 1969 through observations of the maser line at 22 GHz (Cheung et al. 1969). However, since the atmosphere of the Earth is opaque to most other water transitions, it was not until very recently that the low-level rotational transitions were observed successfully. In recent years these transitions have been observed using space-based telescopes like the *Submillimeter Wave Astronomy Satellite* (SWAS Melnick et al. 2000), *Odin* (Frisk et al. 2003; Nordh et al. 2003), the *Infrared Space Observatory* (ISO Kessler et al. 1996) and *Spitzer* (Werner et al. 2004). Of those facilities, only SWAS and *Odin* were capable of detecting the ground-state transition of *ortho*-water at 557 GHz. Also, these two telescopes were the first observatories capable of resolving the line profiles spectrally. The observations of H₂O in outflows with SWAS and *Odin* were summarised in Franklin et al. (2008) and Paper I. The angular resolution of these instruments, when observing the H₂O ($1_{10} - 1_{01}$) line at 557 GHz, were however severely limited ($\sim 4'$ for SWAS and $\sim 2'$ for *Odin*). The spatial resolution of *Odin* allowed only for strip mapping of outflows, where a few selected positions along the flow were observed (Paper I). The situation has significantly improved with the launch of *Herschel* in 2009. It is now possible to observe the H₂O ($1_{10} - 1_{01}$) line at a spatial resolution of $\sim 38''$ (Olberg 2010; Roelfsema et al. 2012) and many other higher frequency transitions at an even better resolution.

Water is a unique probe of warm gas in protostellar environments since its abundance is strongly influenced by the presence of shock waves. As such it is also a tracer of outflow emission, where shocks occur frequently. In the aftermath of a shock, the gaseous water abundance is expected to be enhanced by orders of magnitudes (Kaufman & Neufeld 1996; Bergin et al. 1998; Flower & Pineau des Forêts 2010) and the high abundance is expected to persist for a long time compared to the time it takes for the gas to cool down. Due to its relatively large dipole moment (1.85 Debye) and the large number of available transitions, H₂O has shown to be a valuable probe to understand the heating and cooling processes in outflows.

The chemistry leading to the formation and destruction of water can be considered to operate in three different regimes (see e.g. van Dishoeck et al. 2011, for a recent review). In the low-temperature gas-phase regime, water is predominantly formed through a series of ion-molecule interactions. The H₂O abundance with respect to H₂ is, however, not expected to attain high values in this regime. At the high temperatures

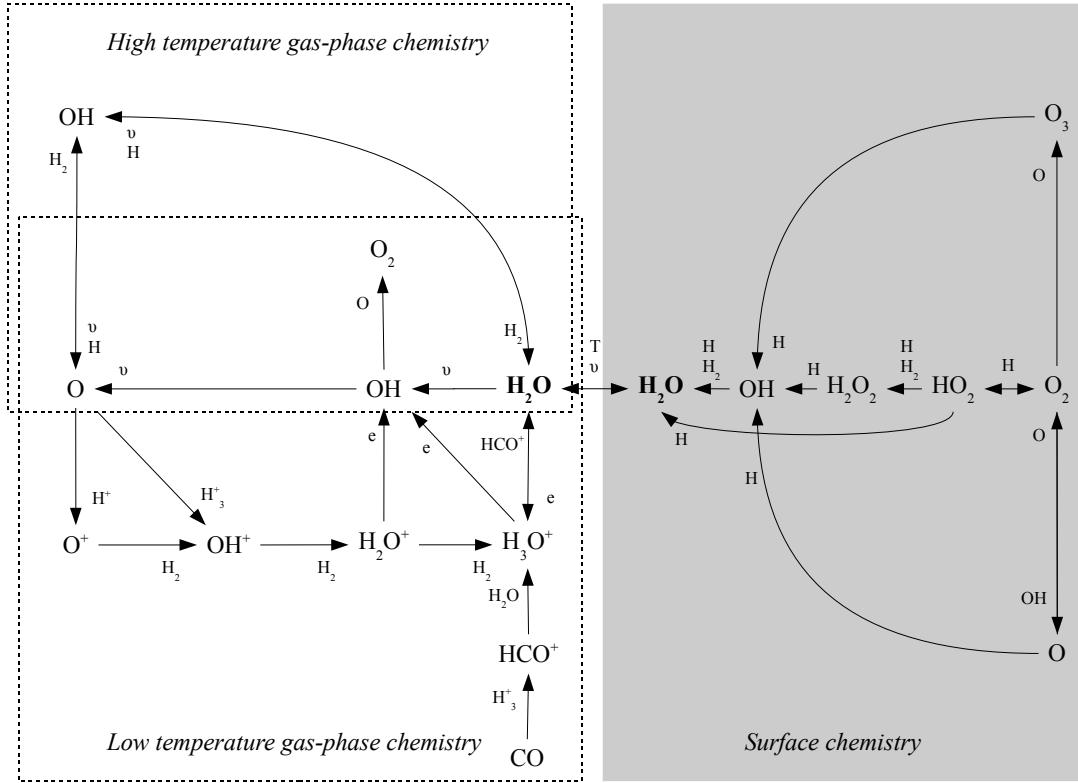


Figure 3.3: The main formation routes important for the destruction and production of H_2O . This figure is adopted from van Dishoeck et al. (2011), where the surface reaction scheme is taken from the study presented by Ioppolo (2010).

that can be reached in shock waves, on the other hand, water production may become efficient due to neutral-neutral reactions in the gas phase and the H_2O abundance with respect to H_2 can be as high as $\sim 10^{-4}$. As mentioned before, also the influence of interstellar grains, has recently become evident and probably all of these regimes are important in outflows where temperatures and densities can vary by order of magnitudes. Thus, the abundance of H_2O is most likely not only determined by the present physical conditions but also conditions that were present in the past. The main reactions leading to the formation of water, either on grains, or in the gas-phase are presented in Fig. 3.3 (adopted from van Dishoeck et al. 2011).

3.2.3 H_2

Molecular hydrogen was detected for the first time the same year as CO, through the detection of several far-ultraviolet (FUV) absorption lines towards the star ξ -Persei (Caruthers 1970). In outflows, however, most studies have focused on observations of the H_2 1–0 S(1) line at $2.12 \mu\text{m}$. Although this line probes gas at very high temperatures

(a few thousand Kelvins, Gautier et al. 1976), it has been particularly useful due to the fact that it can be observed from the ground. Of greater interest in outflow research are, however, the pure rotational transitions in the lowest vibrational state that trace the gas at a lower temperature. With the launch of ISO in 1995, a few of these transitions could be observed for the first time. However, with the mapping capabilities of *Spitzer*, the situation significantly improved and observations of the H₂ 0–0 S(0) to S(7) lines were conducted towards several outflows (Neufeld et al. 2009; Nisini et al. 2010; Giannini et al. 2011, Paper III). From these studies it is clear, that the ortho-to-para ratio of H₂ in most sources is lower than 3. This indicates that the temperature of the shocks is elevated for a limited amount of time and para-to-ortho conversion is only partially in these shocks (see e.g. Neufeld et al. 2006).

Historically, the column density of H₂O has been compared with that of CO, which in turn (assuming a CO/H₂ abundance ratio) gives the H₂O abundance with respect to H₂. Comparison of line profiles and spatial distributions of H₂O and CO has, however, led to the insight that these two molecules not always trace the same gas. Unlike H₂O, the low-*J* transitions of CO seem to trace predominantly the entrained gas component. Instead, H₂ has shown to be a valuable probe, tracing excitation conditions more similar to the ones that pertain to H₂O (see e.g. Santangelo et al. 2012).

3.3 Line profile shapes

3.3.1 Observed line profiles

With the HIFI instrument (de Graauw et al. 2010; Roelfsema et al. 2012), it is for the first time possible to investigate the line profiles of several H₂O lines in detail and to compare those with the profiles of other tracers. Due to the mapping capabilities of *Herschel*, this can be readily done in a region covering the protostellar source, envelope, outflow as well as the quiescent gas component. The observed line profiles reflect the velocity structure of these components, but also the temperature, density and abundance distributions as well as the optical depth.

From the first years of HIFI observations it is obvious that H₂O traces a gas component that largely emits at high velocities with respect to the systemic velocity. High-velocity components previously detected towards L 1448 in CO (Bachiller et al. 1990) stand out in the H₂O spectra (Kristensen et al. 2011) and the H₂O/CO ratio usually increases with higher velocity (although the bulk part of the water emission is at lower velocities like for CO). Franklin et al. (2008) and Kristensen et al. (2011) interpret this to be a consequence of an increase in H₂O abundance with velocity. However, this interpretation has recently been challenged by Nisini et al. (2012) who report a decreasing H₂O/CO ratio at velocities higher than 30–40 km s⁻¹. It has been suggested by these authors that the change in the line ratio rather could be due to a change in temperature and/or density between different velocity regimes. In Fig. 3.4, line profiles of three different species towards L 1448-mm are compared (Nisini et al. 2012). From this comparison it is clear that H₂O does not trace a gas component that moves with a higher

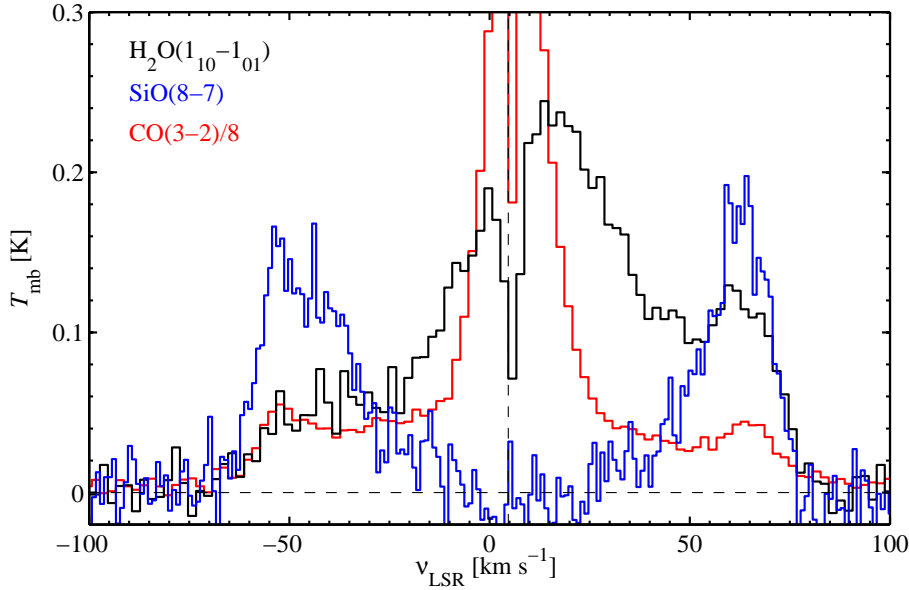


Figure 3.4: Comparison of the line profile shapes observed in H₂O (black), CO (red) and SiO (blue). The figure is adopted from Nisini et al. (2012). The systemic velocity is indicated with a dashed line. These spectra were obtained towards L1448-mm. The outflow wings as well as the high-velocity components are visible in this figure. Also, the CO and H₂O line profiles suffer from self-absorption at $v_{\text{LSR}} = +4.7 \text{ km s}^{-1}$.

velocity than the gas responsible for the CO emission. Furthermore, it is evident that the bulk of the SiO emission originates in the gas that moves at the highest velocity.

3.3.2 Predicted line profiles from shock-models

It is reasonable to assume that a 3D geometry is needed to reproduce the observed line profiles in outflows in a correct way. Nevertheless, recent planar shock modelling has been successful in predicting the overall line shapes of several observed species. When shock speeds are high ($v_s \gtrsim 25 \text{ km s}^{-1}$), sputtering from dust-grains can release enough material to account for the characteristic spike-like profiles observed in SiO, e.g., towards L 1448 (Gusdorf et al. 2008). For CO and H₂O, line profile predictions, computed from shock models, have been presented by Flower & Pineau des Forêts (2010). Wing-like profiles are predicted in these models but they are in this case a consequence of the computed gradient in flow variables. For plane-parallel regions where all variables are kept constant, line profiles will generally not have wing-like shapes (see Paper II). In reality shocks are not 1D, but instead the pressure increases in the inter-shock region leads to the acceleration of material in the transverse direction and this effect is not accounted for in the simulations presented by Flower & Pineau des Forêts (2010). To

directly compare the observations with predicted line profiles one could in principle argue that all of the H₂O emission stems from a confined region close to the apex of the shock but observations do not support this scenario, where the emission for many sources is extended (Tafalla et al. 2012, submitted). For CO, it is evident that entrained material contributes to the shape of the line profiles. However, assuming that the same gas is responsible for the emission in CO and H₂O, one can compare the computed line ratio with observed values (see Paper II).

To model observed line profiles in a correct way, one has to take the full 3D geometry into account as well as the gradients in the flow variables. This modelling approach is, however, yet to be done.

3.4 Individual objects

In this Section, two of the objects (see Paper II & III) discussed in this thesis are presented more thoroughly. HH 54 has been observed extensively, by co-authors of the appended papers, in the past (see e.g. Liseau et al. 1996; Nisini et al. 1996; Giannini et al. 2006) and was also one of the sources targeted by *Odin* (Paper I & II). The source is interesting in the sense that it is a relatively nearby object where the head of the shock is moving essentially towards us. Thus the spatial scales are sufficiently large to be resolved with space-based telescopes like *Herschel*. The outflow emanating from VLA 1623 is also a nearby object but in contrast to HH 54 it is inclined almost face on. This outflow was the target for the mapping observations described in Paper III.

3.4.1 HH 54

HH 54 is a Herbig-Haro object located at a distance of ~ 180 pc (Whittet et al. 1997). It is situated close to the edge of the Chamaeleon II cloud, which is a part of the Chamaeleon cloud complex. This region is a nearby site of ongoing low-mass star formation and contains three prominent dark clouds discovered by Hoffmeister (1962). Several HH objects (HH 52, HH 53 and HH 54) are visible in the region and these objects have been carefully studied in the past (see e.g. Caratti o Garatti et al. 2009). In HH 54, several knots are visible and they move at high velocities towards the observer. However, the nature of the driving source of HH 54 is still not known. Only blue-shifted outflow emission has been detected in the region and several suggestions have been put forward regarding the location of the (proto-) stellar source (see Fig. 3.5). Caratti o Garatti et al. (2009) suggest that IRAS 1500-7658 could be the driving source of HH 54 while arguments for IRAS 12553-7651 (ISO-Cha II 28) being the source are presented in Paper II. The reason for the non-detection of a red-shifted counterpart is not known, but it could be that this part of the outflow is moving out of the cloud where densities are lower. Although the nature of the driving source is not a settled question, HH 54 is an excellent target for an observer. As already mentioned, the source is located relatively nearby and occupies a region that is large enough to be resolved. The shocked region is also virtually free from contamination by other outflows.

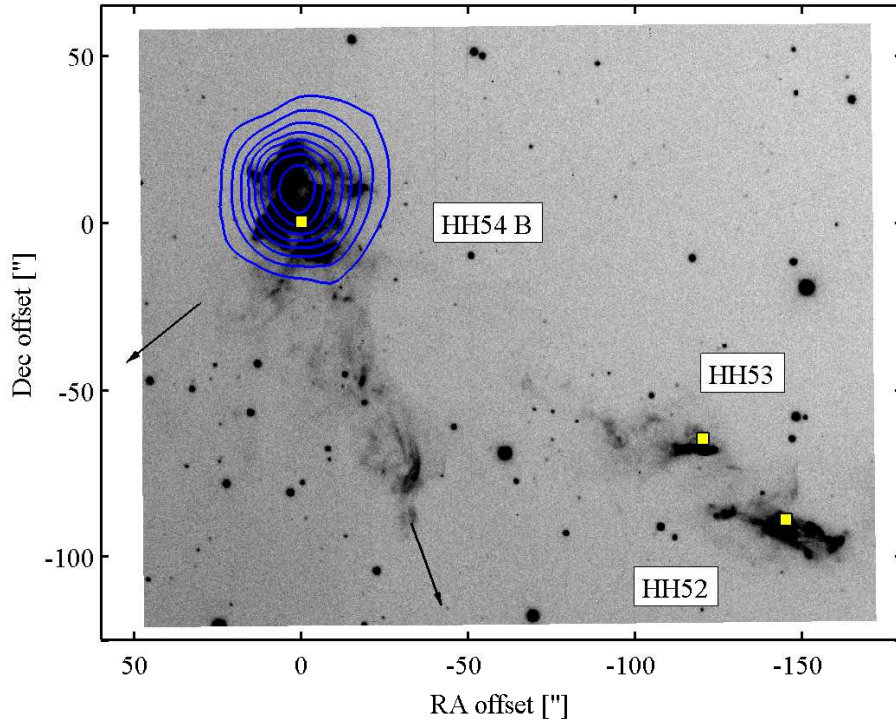


Figure 3.5: Image of the HH 54 region (adopted from Paper II) where the position of the HH 54 B knot is indicated (Sandell et al. 1987). Contours show the CO (10–9) integrated intensity (HIFI) and the colourmap shows the $H\alpha$ image from Caratti o Garatti et al. (2009). The arrows point in the directions of two of the proposed sources of the outflow, viz. IRAS 12553-7651 (south-east) and IRAS 12500-7658 (south).

3.4.2 VLA 1623

VLA 1623 is located in one of the most nearby star-forming clouds L 1688 (Loren et al. 1990) at a distance of ~ 120 pc (Lombardi et al. 2008). It is located close to the ρ Oph A cloud core (see Fig. 3.1), one of the targets for the search of interstellar molecular oxygen carried out in recent years. In the end, it was in this region that O_2 was first detected, by *Odin* (Larsson et al. 2007) and later confirmed by *Herschel* (Liseau et al. 2012). Hydrogen peroxide (H_2O_2) and the hydroperoxyl radical (HO_2) have also recently been detected here (Bergman et al. 2011; Parise et al. 2012). Together with O_2 and OH, they are important constituents of the chemical reaction network leading to the formation of H_2O (see Fig. 3.3).

The central source of the outflow (VLA 1623) was the first to be classified as a Class 0 source (André et al. 1990, 1993), however, also in this case the nature of the exciting source is to some extent a matter of debate. It has been suggested both that the central source is part of a binary system (Looney et al. 2000) and that it is not (Ward-Thompson

et al. 2011; Maury et al. 2012). The outflow has a large projected distance on the sky where the extent in the southeastern direction is 0.5 pc from the central source (Dent et al. 1995). The collimation of the CO outflow has been found to be high (> 10), consistent with what is expected for an outflow of very young age.

Appended papers

4.1 Introduction

The *Odin* satellite, with its 1.1 m diameter mirror, was launched in 2001. The achieved spatial resolution of $\sim 2'$ at 557 GHz was at that time unprecedented and allowed for (strip-) mapping of H₂O in molecular outflows for the first time. This thesis discusses some of the observations carried out towards molecular outflows using first *Odin* and later on *Herschel*. The appended papers are introduced in this Section and the main conclusions that can be drawn from this work are presented in Section 4.2. In Section 4.3, the observational facilities and used data reduction methods are presented. Finally, Section 4.4 includes a brief description of the research projects that I am currently involved in.

4.1.1 Paper I

In Paper I, the observations of shocked gas, carried out with *Odin*, are presented. The aim of this work was to deduce the abundance of H₂O in shocks and to check whether these abundances match recent predictions from shock models. Since the main scientific justification for these observations was to investigate shock chemistry, not only outflows were targeted. In total, fifteen different sources were observed, either towards one position, or towards several positions covering a larger region. Of these sources, 13 were known molecular outflows and two were supernova remnants. In seven of the outflows and in one of the supernova remnants, H₂O was detected.

By measuring the line width and line intensity for each individual source, the column density of H₂O could be inferred using the radiative transfer code RADEX. The density was inferred from CO observations carried out by other authors and the temperatures were taken from previous studies. It should be noted therefore, that the derived H₂O abundances with respect to H₂ (assuming a CO to H₂ ratio of 10^{-4}) reflect also the temperature and the density of regions traced by other species. The derived H₂O abundances for most sources are in fairly close agreement with what one would

expect if all oxygen is converted into water in a shock, i.e., 10^{-5} - 10^{-4} . Comparison between the derived water abundances and mass-loss rates taken from the literature does not show any correlation. On the other hand, there is a correlation between the water abundance and the maximum velocity of the H₂O gas. The sizes of the sources were estimated from comparison with data obtained with the slightly smaller telescope SWAS.

4.1.2 Paper II

In Paper II, previously published observations of HH54 (Paper I) were followed up with new observations acquired with *Odin*, APEX and *Herschel*. The aim of this project was to deduce the relative contribution to the cooling from CO and H₂O and to improve the understanding of the formation of spectral line profiles. Low-*J* CO transitions ranging from CO(2-1) to CO(10-9) as well as the ground state transitions of *o*-H₂O, viz. H₂O(1₁₀ - 1₀₁) and H₂O(2₁₂ - 1₀₁), were observed using APEX and *Herschel*. Complementary observations of the H₂O(1₁₀ - 1₀₁) line were also acquired with *Odin*.

Comparisons with recent planar, isothermal C-shock models with constant density, show that these models do not resemble the observed line profiles shapes. In this paper we instead argue, that the observed line profiles can be accounted for when the geometry is curved instead of planar. The observed CO and H₂O line profiles have a pronounced triangular shape. In the CO line profiles, however, a superimposed additional feature is visible and the spatial extent of the emission responsible for this feature seems to be limited, i.e., unresolved. The H₂O abundance in this region is likely to be low compared to the regions responsible for the overall line shape. The density in the shocked regions is inferred from the CO observations and the H₂O observations are well fit with $X(o\text{-H}_2\text{O}) = 10^{-5}$. The large CO to H₂O cooling rate ratio ($\Lambda(\text{CO})/\Lambda(o\text{-H}_2\text{O}) = 10$) is not in close agreement with recent shock modelling. Nevertheless, the relatively low H₂O abundance led us to conclude that J-shocks may contribute significantly to the emission.

4.1.3 Paper III

In Paper III, *Herschel* observations of the VLA 1623 outflow are discussed. Also in this project, one of the aims was to investigate the water abundance in a molecular outflow. In this case, however, an area covering a large portion of the outflow was mapped using the HIFI and PACS (Poglitsch et al. 2010) instruments. This allowed for the determination of the physical properties of the H₂O outflow as well as investigation of the kinematical information. In fact, this dataset is the first where both the H₂O line profiles are resolved at a high spectral resolution and where the H₂O emitting regions are resolved spatially. The two ground-state transitions of *o*-H₂O were mapped in a region covering the inner 5' of the outflow. In addition to this, several higher energy transitions of both *ortho*- and *para*-H₂O were observed towards two outflow positions showing enhanced emission in CO.

The H₂O data were compared to a grid of RADEX models where the temperature, H₂ density and column density of H₂O is varied. The observed line intensities show that the H₂O regions coincident with the CO emission peaks are warm, i.e., $T \gtrsim 200$ K. The column density of H₂O is inferred to be in the range $3 \times 10^{12} \text{ cm}^{-2}$ to $1 \times 10^{15} \text{ cm}^{-2}$. Observations of purely rotational H₂ lines allow us to derive the temperature and column density of H₂ using population diagram analysis. The population diagrams indicate the presence of two temperature components at ~ 400 K and ~ 1000 K. From comparison of H₂O and H₂, and in agreement with the findings presented by other authors, we conclude that H₂ is likely to be a better tracer of the H₂O emitting gas than CO. Observed line profiles are in agreement with a scenario where the temperature of the H₂O emitting gas is equal to the lower temperature component derived from the *Spitzer* data. Again the geometry of the region may have an important influence on the observed line profile shapes. The water abundance in the northwestern part of the outflow is lower than what is anticipated from recent shock models, viz. $< 10^{-6}$. It can, however, be an order of magnitude higher towards the Herbig-Haro object HH 313 A.

A position-velocity diagram shows a tendency that the velocity of the gas increases with distance from the central source. This pattern has previously been observed towards several outflow sources in CO, but to our knowledge, this is the first time that this is seen also for the H₂O emitting gas.

The information obtained from *Herschel* and *Spitzer* observations allow us to derive the physical parameters of the flow. Although high uncertainties are involved in these calculations, we derive similar values for the momentum rate, energy and mechanical luminosity as when CO is the molecular tracer used.

4.1.4 Paper IV

The investigation of the physical parameters presented in Paper III was based on the observation of one object. Also, only one of the outflow lobes was fully covered by the H₂O observations. In this letter, we extend the analysis to also include the two other outflows that have been mapped with HIFI, viz. L 1448 and L 1157. The estimates based on CO observations were taken from the literature and the inferred values were updated using the most recent method to correct for the inclination of the outflows. The gas responsible for the H₂O emission and the gas, which is responsible for the H₂ emission, have similar spatial distributions. In addition to this, recent findings also indicate that the physical conditions are similar. We therefore estimate the mass of the H₂O emitting gas, from H₂ observations carried out with *Spitzer*. Regardless of whether CO or H₂O and H₂ observations are used to estimate the momentum rate and mechanical luminosity, we derive similar values for these quantities.

4.2 Conclusions and summary of the results

The H₂O data discussed in this thesis were collected over a period of ten years. Not unexpectedly, insights when it comes to the excitation of H₂O have been assimilated

during this period of time. Prior to the SWAS and *Odin* missions, the lowest rotational transitions of H₂O had never been observed. Therefore, at the time when the first observations of the 557 GHz line were carried out, less was known about the excitation and de-excitation conditions of H₂O in molecular outflows. In recent years, however, substantial work has been done in order to increase our understanding of H₂O in molecular outflows. In this section the main conclusions that can be drawn from the work presented in this thesis are presented.

Paper I:

- We present H₂O detections at 557 GHz towards seven molecular outflows and one supernova remnant. Together with previously published ISO and SWAS results, this study confirms the presence of thermal H₂O emission from molecular outflows. Noteworthy, in comparison with the later papers appended to this thesis, is that the derived H₂O abundances in general are higher than what was later inferred from observations using *Herschel* (see e.g. Vasta et al. 2012; Santangelo et al. 2012, Paper III). One reason for this is the low temperatures and densities that were assumed when analysing the data. It should therefore be noted that this is not necessarily the case. Observations of only one rotational transition do not allow us to determine these quantities in a reliable way.
- There is a correlation between the H₂O abundance and the maximum velocity of outflowing gas. Also, recent *Herschel* observations of 29 low-mass sources show that there is a strong correlation between the H₂O line flux and the maximum detected velocity of the flow (Kristensen et al. 2012). One can from this, however, not draw the conclusion that the H₂O abundance is higher in regions where the velocity is high. The correlation merely shows that the velocity of the flow is contributing to the overall H₂O abundance in the observed region. The H₂O abundance is also expected to persist for a long time after the passage of a shock.

Paper II:

- We compare observations of shocked H₂O gas in HH 54 with recent planar shock models. This study shows, that the line profiles cannot be fully explained when having a planar geometry. Instead we suggest that the geometry can play an important role for the observed line profiles, since a 2D geometry can completely account for observed shapes. It has to be emphasised that we do not claim that the region is isothermal and/or has a constant density. Gradients in the flow variables can contribute to the shape as well.
- A bump-like feature is detected in several of the CO line profiles detected towards HH 54. This emission likely originates in a region of size $\sim 10''$, where the density is lower and the temperature is higher than in the surrounding region. This could indicate the presence of an under-dense jet.

- The estimated cooling rate ratio of $\Lambda(\text{CO})/\Lambda(o\text{-H}_2\text{O}) \gg 1$ is unexpectedly high. Although the low value of the derived H_2O abundance suggests the presence of J-shocks, CO to H_2O line ratios are far from what would be expected according to both J- and C-shock models.

Paper III:

- The mapping observations show a variety of line profile shapes in the observed region covering the VLA 1623 outflow. From comparison with LVG models we conclude that the gas responsible for the H_2O emission is warm ($T > 200$ K) and that the H_2O abundance is remarkably low ($X(\text{H}_2\text{O}) < 10^{-5}$). In the majority of the positions in the map, the profiles are similar to what is commonly attributed to infall. However, in this case, this type of profiles is observed over a larger area. The line shapes can be explained by the observed velocity structure of the region (from other tracers), and may therefore not indicate the existence of a large-scale infall.
- The estimated *ortho-to-para* ratio for H_2O is lower than 3, but still, this number falls within the error of the estimate. Therefore, we cannot draw any firm conclusions what regards the origin of the H_2O that is observed. Nevertheless it is interesting that the derived values are low and in close agreement with what has been measured for H_2 in molecular outflows (Neufeld et al. 2009). The low *ortho-to-para* values could indicate that the temperature when the formation occurred was very low (of the order 20 K). Adhering to this line of argument, it would in that case indicate that an important source of H_2O in this outflow is from the dust grains.
- When estimating the physical parameters of the flow, we arrive at the conclusion that the force driving the outflow is the same and independent of which molecular tracer that is used (CO or H_2O and H_2). The dynamical time scale of only ~ 700 years confirms that the source is likely to be very young. The reason for this could be that, also for H_2O , transverse gas motions and entrainment play important roles.
- At low velocities, the position-velocity diagram reveals a trend where the velocity increases with distance from the central source. This is consistent with what has previously been observed in CO and is what one expects to observe in a momentum driven flow.

Paper IV:

- The inferred values for momentum rate and mechanical luminosity are independent of whether we use CO or H_2O and H_2 as tracers of the outflow emission. This result is perhaps not entirely unexpected, but highlights that previous estimates are still valid. It is also likely that it is the same ejection mechanism that

is responsible for the characteristics of the gas traced by the different molecular species. The three outflows are all very young with dynamic time-scales of less than or about 10^3 years.

In summary, the work presented in this thesis has mainly contributed to the understanding of interstellar shock waves. Although H_2O is an important coolant, its role in the star-formation process is yet not fully understood. The emission from H_2O predominantly traces the outflowing gas, not the gas that finally ends up in the stellar system. H_2O has also been shown to be much more dilute than predicted and as such it contributes less to the cooling of the shocked gas than what was previously expected.

4.3 Observations and data reduction methods

Although complementary observations have been carried out with different ground-based facilities, this thesis is primarily based on data acquired with the space-based telescopes *Odin* and *Herschel* (see Fig. 4.1). The *Odin* observations are discussed in Papers I & II and the *Herschel* observations in Papers II, III & IV. This section includes a brief description of these facilities and the scientific instruments they are equipped with.

4.3.1 Odin

The *Odin* sub-millimetre wave satellite was launched in February 2001 (Nordh et al. 2003). During the first years of operation it was shared between the fields of astronomy and aeronomy, however, today more than ten years later it is mainly used for aeronomy research. It is situated in a polar orbit at an altitude of 600 km. Out of the 96-minute orbit, 61 minutes can be used for astronomical observations, while the occultation periods of 35 minutes can be used for calibration using atmospheric spectral lines. From Jupiter mappings, the main beam efficiency of the 1.1 m telescope was measured to be 90% (Hjalmarson et al. 2003). Three different spectrometers are situated onboard the spacecraft. One of them is an acousto-optical spectrometer (AOS), with a fixed channel spacing of 620 kHz while the other two are auto-correlators (AC1, AC2) that can be used in different modes. The frequency coverages are 119, 486 – 504 and 541 – 581 GHz. The beam size at 557 GHz is estimated to be $126''$.

4.3.2 Herschel

The *Herschel* Space Observatory was launched in May 2009 and is believed to be in operation until early 2013. To provide a stable thermal and radiation environment it has been injected into a halo orbit around the second Lagrange point (L2). L2 is one of the five points where the gravity from two larger bodies (in this case the Earth and the Sun) affects a small body in such a way that it can rotate together with them. Three different instruments covering different wavelength regions are operating onboard the



Figure 4.1: *Left panel:* Artist's impression of the *Herschel* spacecraft. Credits: ESA/AOES Medialab; background: Hubble Space Telescope image (NASA/ESA/STScI). *Right panel:* Artist's impression of the *Odin* satellite.

spacecraft. The Spectral and Photometric Imaging Receiver (SPIRE) uses bolometer arrays at 250, 350 and 500 μm , the Photodetector Array Camera and Spectrometer (PACS) provides the user with imaging capabilities at 60 – 210 μm . Although it is possible to do spectroscopy with PACS and SPIRE, it is the third instrument, HIFI, which has the high-resolution capabilities. HIFI operates in the frequency ranges, 480 – 1250 GHz (625 – 240 μm) and 1410 – 1910 GHz (213 – 157 μm), split in seven different bands. In total there are four spectrometers in the instrument: two Wide Band Acousto Optical Spectrometers (WBS) and two High Resolution Autocorrelation Spectrometers (HRS). One of the two versions of each spectrometer pair observes in horizontal polarisation whereas the other one observes the vertical component. This is useful for some astronomical interpretations but it also gives redundancy to the system in case of failure of one or two spectrometers. The data are obtained in both sidebands.

The data discussed in Papers II, III & IV were acquired within the framework of the Water In Star-forming regions with *Herschel* (WISH¹) guaranteed time key program

¹<http://www.strw.leidenuniv.nl/WISH/>

(van Dishoeck et al. 2011). In this program, about 80 sources, ranging from low- to high-mass, and young (collapsing clouds) to old (protostellar disks) objects are observed. The aim of the program is to investigate the nature of young stellar objects and their environments using primarily the H_2O molecule as a tracer of these regions. One of the seven different subprograms in this large collaboration is the outflow program where three different sources (L 1157, L 1448 and VLA 1623) have been mapped in the ground-state transitions of *o*- H_2O using HIFI and PACS (Paper III; Paper IV; Nisini et al. 2012). In addition to this, a line survey has been conducted towards selected positions in 25 Class 0 and Class I sources (Tafalla et al. 2012, submitted). The aim of this project has been to investigate the physical conditions in the regions responsible for the water emission, i.e., distribution and abundances in comparison with up to date shock models. Also, valuable kinematical information from the resolved line profiles provided by the HIFI instrument has been obtained.

4.3.3 Data reduction methods

All data acquired with *Herschel* are processed to a certain level and stored in the *Herschel Science Archive* (HSA). The observations have a proprietary period of 6 months (12 months for data acquired during the first year of observations) and are then publicly available to the scientific community. The initial inspection of the *Herschel* data discussed in this thesis was done using the *Herschel Interactive Processing Environment* (HIPE, Ott 2010), but subsequent data reduction and analysis was done using other software (in collaboration with other members of the outflow team). Software such as XS, IDL, Matlab and CLASS was frequently used to generate publishable data products. For the data discussed in Paper III and IV, a Statistical Image Deconvolution (SID) technique (Rydbeck 2008) was used to improve the spatial resolution of the HIFI map.

4.4 Current and future research projects

4.4.1 Herschel observations of the shocked gas in HH 54

To understand outflows we also need to understand the nature of interstellar shock waves and the role of water and other molecules. Since the shocked gas in HH 54 is relatively nearby and occupies a confined region in space, we have chose to continue observing this target using *Herschel* and APEX. In 2011, we submitted a proposal to carry out spectroscopic observations of the rotational H_2O and CO transitions that can be observed with PACS, and SPIRE. In addition to this, selected transitions were to be observed with HIFI. This project (OT2_pbjerkel1) was awarded 4.7 hours of observing time. Complementing these observations, we have also mapped the HH 54 region in CO (3–2) with APEX.

As for the *Herschel* observations, all three instruments will be used and to date the HIFI and PACS data have been collected. The aims of the project were several. From

observations of the rotational CO lines (up to $J_{\text{up}} = 49$) we aim at obtaining spatial information on the excitation conditions. The CO lines that will be covered by PACS and SPIRE probe different physical components in the shocked region (see Paper III). In addition to this, also the OI lines at 63 and 145 μm and several H₂O lines fall into the covered wavelength region. As already mentioned in this thesis, several studies indicate that the low- J CO emission is not co-spatial with the H₂O emission. The assumption that CO and H₂O trace the same gas component in this case therefore needs to be checked. In order to constrain the origin of the bullet emission and to obtain kinematical information, we also observe CO (3–2), CO (4–3), CO (15–14) and H₂O (2₁₂ – 1₀₁) with HIFI and APEX. For the HIFI observations we adopted a strategy where we only observe one position but for the lower J transitions CO (3–2) and CO (4–3) we instead chose to map the HH 54 region. The CO (3–2) data are already collected, and the bullet feature was detected with a high signal-to-noise ratio. Since the APEX-3 receiver is now released for public use, we have sent in a proposal to map also the CO (4–3) emission. By comparing the CO observations to *Spitzer* observations, with high angular resolution, we also aim at determining the CO abundance to a great accuracy.

4.4.2 H₂O mapping of the ρ Ophiuchi A cloud

Just like the Chamaeleon clouds, the ρ Ophiuchi A cloud is located relatively nearby (~ 120 pc) which allows for spatially resolved observations with *Herschel*. Unlike the case with HH 54, however, this region contains multiple and different environments. The mapping observations presented in Paper III and IV only covered the outflow emanating from VLA 1623. However, residing slightly north from this region is the ρ Oph A cloud core which is illuminated from the rear side by B type stars.

Therefore, in a *Herschel* program led by René Liseau, the available H₂O maps will be extended to cover also the regions surrounding the VLA 1623 outflow. The H₂O map will be extended to cover a 4.5' by 5.5' region and simultaneously, also the NH₃ (1₀ - 0₀) line will be observed in the other sideband. In addition to this, the OI lines at 63 and 145 μm as well as the 179 and 180 μm H₂O lines will be mapped in a region stretching from VLA 1623 to the north of the ρ Oph A core. The aim of this project is to conduct further investigations of the chemistry and physics in these regions. When this thesis is sent to the printer, the observations with *Herschel* has just started and the data will be analysed in the near future.

Bibliography

- Adams, F. C. & Laughlin, G. 1997, *Reviews of Modern Physics*, 69, 337
- Ambartsumian, V. A. 1947, *Armenian Academy of Science*
- Ambartsumian, V. A. 1955, *The Observatory*, 75, 72
- André, P., Martin-Pintado, J., Despois, D., & Montmerle, T. 1990, *A&A*, 236, 180
- André, P. & Montmerle, T. 1994, *ApJ*, 420, 837
- André, P., Ward-Thompson, D., & Barsony, M. 1993, *ApJ*, 406, 122
- Arce, H. G., Shepherd, D., Gueth, F., et al. 2007, in *Protostars and Planets V*, ed. B. Reipurth, D. Jewitt, & K. Keil, 245–260
- Bachiller, R., Martin-Pintado, J., Tafalla, M., Cernicharo, J., & Lazareff, B. 1990, *A&A*, 231, 174
- Bachiller, R., Pérez Gutiérrez, M., Kumar, M. S. N., & Tafalla, M. 2001, *A&A*, 372, 899
- Bachiller, R. & Tafalla, M. 1999, in *NATO ASIC Proc. 540: The Origin of Stars and Planetary Systems*, ed. C. J. Lada & N. D. Kylafis, 227
- Banerjee, R. & Pudritz, R. E. 2006, *ApJ*, 641, 949
- Barrado y Navascués, D. & Martín, E. L. 2003, *AJ*, 126, 2997
- Bergin, E. A., Neufeld, D. A., & Melnick, G. J. 1998, *ApJ*, 499, 777
- Bergman, P., Parise, B., Liseau, R., et al. 2011, *A&A*, 531, L8+
- Burnham, S. W. 1890, *MNRAS*, 51, 94
- Cabrit, S. & Bertout, C. 1992, *A&A*, 261, 274
- Cabrit, S., Edwards, S., Strom, S. E., & Strom, K. M. 1990, *ApJ*, 354, 687

- Cabrit, S., Raga, A., & Gueth, F. 1997, in IAU Symposium, Vol. 182, Herbig-Haro Flows and the Birth of Stars, ed. B. Reipurth & C. Bertout, 163–180
- Caratti o Garatti, A., Eisloffel, J., Froebrich, D., et al. 2009, *A&A*, 502, 579
- Carruthers, G. R. 1970, *ApJ*, 161, L81
- Cheung, A. C., Rank, D. M., Townes, C. H., Thornton, D. D., & Welch, W. J. 1969, *Nature*, 221, 626
- Codella, C., Lefloch, B., Ceccarelli, C., et al. 2010, *A&A*, 518, L112+
- Crapsi, A., van Dishoeck, E. F., Hogerheijde, M. R., Pontoppidan, K. M., & Dullemond, C. P. 2008, *A&A*, 486, 245
- Crutcher, R. M., Wandelt, B., Heiles, C., Falgarone, E., & Troland, T. H. 2010, *ApJ*, 725, 466
- Daniel, F., Dubernet, M., Picaud, F., & Grosjean, A. 2010, *A&A*, 517, A13+
- Daniel, F., Dubernet, M.-L., & Grosjean, A. 2011, *A&A*, 536, A76
- de Graauw, T., Helmich, F. P., Phillips, T. G., et al. 2010, *A&A*, 518, L6+
- Dent, W. R. F., Matthews, H. E., & Walther, D. M. 1995, *MNRAS*, 277, 193
- Downes, T. P. & Cabrit, S. 2007, *A&A*, 471, 873
- Draine, B. T. 1980, *ApJ*, 241, 1021
- Dubernet, M.-L., Daniel, F., Grosjean, A., et al. 2006, *A&A*, 460, 323
- Dubernet, M.-L., Daniel, F., Grosjean, A., & Lin, C. Y. 2009, *A&A*, 497, 911
- Einstein, A. 1917, *Physikalische Zeitschrift*, 18, 121
- Falgarone, E., Troland, T. H., Crutcher, R. M., & Paubert, G. 2008, *A&A*, 487, 247
- Faure, A., Crimier, N., Ceccarelli, C., et al. 2007, *A&A*, 472, 1029
- Flower, D. R. & Pineau des Forêts, G. 2010, *MNRAS*, 406, 1745
- Franklin, J., Snell, R. L., Kaufman, M. J., et al. 2008, *ApJ*, 674, 1015
- Fridlund, C. V. M. & Liseau, R. 1998, *ApJ*, 499, L75+
- Frisk, U., Hagström, M., Ala-Laurinaho, J., et al. 2003, *A&A*, 402, L27
- Gautier, III, T. N., Fink, U., Larson, H. P., & Treffers, R. R. 1976, *ApJ*, 207, L129
- Giannini, T., McCoey, C., Nisini, B., et al. 2006, *A&A*, 459, 821

- Giannini, T., Nisini, B., Neufeld, D., et al. 2011, *ApJ*, 738, 80
- Goldsmith, P. F. & Langer, W. D. 1999, *ApJ*, 517, 209
- Greene, T. P., Wilking, B. A., Andre, P., Young, E. T., & Lada, C. J. 1994, *ApJ*, 434, 614
- Gueth, F., Guilloteau, S., & Bachiller, R. 1996, *A&A*, 307, 891
- Gusdorf, A., Cabrit, S., Flower, D. R., & Pineau Des Forêts, G. 2008, *A&A*, 482, 809
- Haro, G. 1952, *ApJ*, 115, 572
- Hartigan, P., Bally, J., Reipurth, B., & Morse, J. A. 2000, *Protostars and Planets IV*, 841
- Herbig, G. H. 1950, *ApJ*, 111, 11
- Herczeg, G. J., Karska, A., Bruderer, S., et al. 2012, *A&A*, 540, A84
- Hirano, N., Ho, P. P. T., Liu, S.-Y., et al. 2010, *ApJ*, 717, 58
- Hjalmarson, Å., Frisk, U., Olberg, M., et al. 2003, *A&A*, 402, L39
- Hoffmeister, C. 1962, *ZAp*, 55, 290
- Hollenbach, D. & Salpeter, E. E. 1971, *ApJ*, 163, 155
- Ioppolo, S. 2010, PhD thesis, Ph. D. thesis, University of Leiden (2010)
- James, H. M. & Coolidge, A. S. 1938, *ApJ*, 87, 438
- Justtanont, K., Bergman, P., Larsson, B., et al. 2005, *A&A*, 439, 627
- Kaufman, M. J. & Neufeld, D. A. 1996, *ApJ*, 456, 611
- Kessler, M. F., Steinz, J. A., Anderegg, M. E., et al. 1996, *A&A*, 315, L27
- Königl, A. & Pudritz, R. E. 2000, *Protostars and Planets IV*, 759
- Kristensen, L. E., van Dishoeck, E. F., Bergin, E. A., et al. 2012, *ArXiv e-prints*
- Kristensen, L. E., van Dishoeck, E. F., Tafalla, M., et al. 2011, *A&A*, 531, L1+
- Lada, C. J. 1987, in *IAU Symposium, Vol. 115, Star Forming Regions*, ed. M. Peimbert & J. Jugaku, 1–17
- Lada, C. J. & Lada, E. A. 2003, *ARA&A*, 41, 57
- Larsson, B., Liseau, R., Pagani, L., et al. 2007, *A&A*, 466, 999
- Lee, C.-F., Mundy, L. G., Stone, J. M., & Ostriker, E. C. 2002, *ApJ*, 576, 294
- Linke, R. A., Frerking, M. A., & Thaddeus, P. 1979, *ApJ*, 234, L139

- Liseau, R., Ceccarelli, C., Larsson, B., et al. 1996, *A&A*, 315, L181
- Liseau, R., Goldsmith, P. F., Larsson, B., et al. 2012, *A&A*, 541, A73
- Liseau, R. & Justtanont, K. 2009, *A&A*, 499, 799
- Livio, M. 2004, *Baltic Astronomy*, 13, 273
- Lombardi, M., Lada, C. J., & Alves, J. 2008, *A&A*, 489, 143
- Looney, L. W., Mundy, L. G., & Welch, W. J. 2000, *ApJ*, 529, 477
- Loren, R. B., Wootten, A., & Wilking, B. A. 1990, *ApJ*, 365, 269
- Machida, M. N., Inutsuka, S.-i., & Matsumoto, T. 2008, *ApJ*, 676, 1088
- Maercker, M., Schöier, F. L., Olofsson, H., Bergman, P., & Ramstedt, S. 2008, *A&A*, 479, 779
- Mannings, V., Boss, A., & Russell, S. 2000, *Protostars and Planets IV*
- Mardones, D., Myers, P. C., Tafalla, M., et al. 1997, *ApJ*, 489, 719
- Masson, C. R. & Chernin, L. M. 1993, *ApJ*, 414, 230
- Masunaga, H. & Inutsuka, S. 2000, *ApJ*, 531, 350
- Mathis, J. S., Rumpl, W., & Nordsieck, K. H. 1977, *ApJ*, 217, 425
- Maury, A., Ohashi, N., & André, P. 2012, *A&A*, 539, A130
- Melnick, G. J., Stauffer, J. R., Ashby, M. L. N., et al. 2000, *ApJ*, 539, L77
- Mihalas, D. 1978, *Stellar atmospheres /2nd edition/*, ed. Hevelius, J.
- Motte, F. & André, P. 2001, *A&A*, 365, 440
- Neufeld, D. A. & Melnick, G. J. 1991, *ApJ*, 368, 215
- Neufeld, D. A., Melnick, G. J., Sonnentrucker, P., et al. 2006, *ApJ*, 649, 816
- Neufeld, D. A., Nisini, B., Giannini, T., et al. 2009, *ApJ*, 706, 170
- Nisini, B., Benedettini, M., Giannini, T., et al. 1999, *A&A*, 350, 529
- Nisini, B., Giannini, T., Neufeld, D. A., et al. 2010, *ApJ*, 724, 69
- Nisini, B., Lorenzetti, D., Cohen, M., et al. 1996, *A&A*, 315, L321
- Nisini, B., Santangelo, G., Antonucci, S., et al. 2012, *ArXiv e-prints*
- Nordh, H. L., von Schéele, F., Frisk, U., et al. 2003, *A&A*, 402, L21

- Olberg, M. 2010, Technical Note: ICC/2010-nnn, v1.1, 2010-11-17
- Ott, S. 2010, in *Astronomical Society of the Pacific Conference Series*, Vol. 434, *Astronomical Data Analysis Software and Systems XIX*, ed. Y. Mizumoto, K.-I. Morita, & M. Ohishi, 139–+
- Parise, B., Bergman, P., & Du, F. 2012, *A&A*, 541, L11
- Pillbratt, G. L., Riedinger, J. R., Passvogel, T., et al. 2010, *A&A*, 518, L1+
- Poglitsch, A., Waelkens, C., Geis, N., et al. 2010, *A&A*, 518, L2+
- Pudritz, R. E., Wilson, C. D., Carlstrom, J. E., et al. 1996, *ApJ*, 470, L123+
- Reipurth, B., Jewitt, D., & Keil, K. 2007, *Protostars and Planets V*
- Ridge, N. A. & Moore, T. J. T. 2001, *A&A*, 378, 495
- Rieke, G. H. & Lebofsky, M. J. 1985, *ApJ*, 288, 618
- Roelfsema, P. R., Helmich, F. P., Teyssier, D., et al. 2012, *A&A*, 537, A17
- Rybicki, G. B. & Hummer, D. G. 1991, *A&A*, 245, 171
- Rybicki, G. B. & Lightman, A. P. 1979, *Radiative processes in astrophysics*, ed. Rybicki, G. B. & Lightman, A. P.
- Rydbeck, G. 2008, *ApJ*, 675, 1304
- Sandell, G., Zealey, W. J., Williams, P. M., Taylor, K. N. R., & Storey, J. V. 1987, *A&A*, 182, 237
- Santangelo, G., Nisini, B., Giannini, T., et al. 2012, *A&A*, 538, A45
- Santiago-García, J., Tafalla, M., Johnstone, D., & Bachiller, R. 2009, *A&A*, 495, 169
- Schöier, F. L., van der Tak, F. F. S., van Dishoeck, E. F., & Black, J. H. 2005, *A&A*, 432, 369
- Shang, H., Allen, A., Li, Z.-Y., et al. 2006, *ApJ*, 649, 845
- Shang, H., Li, Z.-Y., & Hirano, N. 2007, *Protostars and Planets V*, 261
- Shu, F. H., Adams, F. C., & Lizano, S. 1987, *ARA&A*, 25, 23
- Shu, F. H., Najita, J. R., Shang, H., & Li, Z. 2000, *Protostars and Planets IV*, 789
- Shu, F. H., Ruden, S. P., Lada, C. J., & Lizano, S. 1991, *ApJ*, 370, L31
- Snell, R. L. 1987, in *IAU Symposium*, Vol. 115, *Star Forming Regions*, ed. M. Peimbert & J. Jugaku, 213–236

- Snell, R. L., Loren, R. B., & Plambeck, R. L. 1979, in Bulletin of the American Astronomical Society, Vol. 11, Bulletin of the American Astronomical Society, 713–+
- Snell, R. L., Loren, R. B., & Plambeck, R. L. 1980, *ApJ*, 239, L17
- Sofia, U. J. & Meyer, D. M. 2001, *ApJ*, 554, L221
- Spitzer, Jr., L. 1949, Leaflet of the Astronomical Society of the Pacific, 5, 336
- Stahler, S. W. 1994, *ApJ*, 422, 616
- Stahler, S. W. & Palla, F. 2005, *The Formation of Stars* (The Formation of Stars, by Steven W. Stahler, Francesco Palla, pp. 865. ISBN 3-527-40559-3. Wiley-VCH, January 2005.)
- Stahler, S. W., Shu, F. H., & Taam, R. E. 1980, *ApJ*, 241, 637
- Tafalla, M., Liseau, R., Nisini, B., et al. 2012, *A&A*, submitted
- Tafalla, M., Mardones, D., Myers, P. C., et al. 1998, *ApJ*, 504, 900
- Tafalla, M., Santiago-García, J., Hacar, A., & Bachiller, R. 2010, *A&A*, 522, A91
- Tielens, A. G. G. M. 2005, *The Physics and Chemistry of the Interstellar Medium*
- Troland, T. H. & Crutcher, R. M. 2008, *ApJ*, 680, 457
- van der Tak, F. F. S., Black, J. H., Schöier, F. L., Jansen, D. J., & van Dishoeck, E. F. 2007, *A&A*, 468, 627
- van Dishoeck, E. F. & Black, J. H. 1987, in *NATO ASIC Proc. 210: Physical Processes in Interstellar Clouds*, ed. G. E. Morfill & M. Scholer, 241–274
- van Dishoeck, E. F., Kristensen, L. E., Benz, A. O., et al. 2011, *PASP*, 123, 138
- Vasta, M., Codella, C., Lorenzani, A., et al. 2012, *A&A*, 537, A98
- Ward-Thompson, D., Kirk, J. M., Greaves, J. S., & André, P. 2011, ArXiv e-prints
- Werner, M. W., Roellig, T. L., Low, F. J., et al. 2004, *ApJS*, 154, 1
- Whittet, D. C. B., Prusti, T., Franco, G. A. P., et al. 1997, *A&A*, 327, 1194
- Wilson, R. W., Jefferts, K. B., & Penzias, A. A. 1970, *ApJ*, 161, L43+
- Wirström, E. S., Bergman, P., Black, J. H., et al. 2010, *A&A*, 522, A19+
- Wu, Y., Wei, Y., Zhao, M., et al. 2004, *Catalogue of high velocity molecular outflows (Update)* (Wu+ 2004)
- Zuckerman, B., Kuiper, T. B. H., & Rodriguez Kuiper, E. N. 1976, *ApJ*, 209, L137

[Some pages are omitted from this version of the thesis.]